

Spatio-temporal variability of zooplankton standing stock in
eastern Arabian Sea inferred from ADCP backscatter
measurements

Ranjan Kumar Sahu, P. Amol, D.V. Desai, S.G. Aparna, D. Shankar

August 23, 2024

Abstract

We use acoustic Doppler current profiler (ADCP) backscatter measurements to map the spatio-temporal variation of zooplankton standing stock in the eastern Arabian Sea (EAS). The ADCP moorings were deployed at seven locations on the continental slope off the west coast of India; we use data from October 2017 to December 2023. The 153.3 kHz ADCP uses backscatter from sediments or organisms such as copepods, ctenophores, salps and amphipods greater than 1 cm to calculate current profile. The backscatter is obtained from echo intensity using RSSI conversion factor after doing necessary calibrations. The conversion from backscatter to biomass is based on volumetric zooplankton sampling at the respective locations. Analysis of the data over 24 – 120 m shows that the backscatter and zooplankton biomass decrease from the upper ocean (215 m g^{-3} biomass contour) to the lower depths. Changes are observed in the seasonal variation of the monthly

¹² climatology of zooplankton standing stock (integral of the biomass over 24 – 120 m water column)
¹³ as we move to poleward along the slope in EAS. The range of variation of standing stock is lowest
¹⁴ at Kanyakumari, followed by Okha, which lie at the southern and northern boundary of the EAS,
¹⁵ respectively. Complementary variables are used to explain the processes leading to growth or decay
¹⁶ of zooplankton biomass.

₁₇ **1 Introduction**

₁₈ **1.1 Background**

₁₉ Zooplankton plays a vital role in food web of pelagic ecosystem by enabling the hierarchical trans-
₂₀ port of organic matter from primary producers to higher trophic levels impacting the fish population
₂₁ and the carbon pump of the deep ocean [Ohman and Hirche, 2001, Le Qu et al., 2016]. They are
₂₂ presumably the largest migrating organisms in terms of biomass [Hays, 2003] which occurs in diel
₂₃ vertical migration (DVM). Zooplanktons depend not only on phytoplankton but other environ-
₂₄ mental parameters (e.g. Mixed layer depth, insolation, Oxygen, thermocline, nutrient availability,
₂₅ chlorophyll concentration and daily primary production). The biological productivity of the ocean
₂₆ is essentially connected with physics and chemistry [Subrahmanyam, 1959, Ryther et al., 1966,
₂₇ Qasim, 1977, Nair, 1970, Banse, 1995, McCreary et al., 2009, Vijith et al., 2016, Amol et al., 2020].
₂₈ The dynamic ocean results in varying physico-chemical properties, leading to bloom and growth of
₂₉ planktons in favourable conditions. The changes are strongly influenced by the seasonal cycle in
₃₀ the North Indian Ocean (NIO; north of 5 °N of Indian Ocean). The eastern boundary of Arabian
₃₁ Sea contains the West India Coastal Current (WICC; [Patil et al., 1964, Ramamirtham and Murty,
₃₂ 1965, Banse, 1968, Shetye et al., 1991, McCreary Jr et al., 1993, Shankar and Shetye, 1997, Shetye
₃₃ and Gouveia, 1998, Maheswaran et al., 2000, Amol et al., 2014, Chaudhuri et al., 2020, 2021])
₃₄ which reverses seasonally, flowing poleward (equatorward) during November to February (June to
₃₅ September).
₃₆ The direct consequence of this reversal is the seasonal cycle of thermocline, oxycline and thick-
₃₇ ness of mixed Layer Depth (MLD) induced by upwelling favourable conditions in summer and down-
₃₈ welling favourable conditions in winter in eastern Arabian Sea (EAS). Further, the phytoplankton

39 biomass and chlorophyll concentration changes with the season [Subrahmanyam and Sarma, 1960,
40 Banse, 1968, Lévy et al., 2007, Vijith et al., 2016]. Upwelling in summer monsoon leads to maximum
41 chlorophyll growth in the entire EAS [Banse, 1968, Banse and English, 2000, McCreary et al., 2009,
42 Hood et al., 2017, Shi and Wang, 2022]. During winter monsoon, the convective mixing induced
43 winter mixed layer [Shetye et al., 1992, Madhupratap et al., 1996b, Lévy et al., 2007, Vijith et al.,
44 2016, Shankar et al., 2016, Keerthi et al., 2017, Shi and Wang, 2022] results in winter chlorophyll
45 peak in northern EAS (NEAS) while the downwelling Rossby waves modulate chlorophyll along the
46 southern EAS (SEAS) albeit limited to coast and islands [Amol et al., 2020].

47 The zooplankton grazing peak is instantaneous with no time delay from peak phytoplankton
48 production [Li et al., 2000, Barber et al., 2001], but its population growth lags [Rehim and Imran,
49 2012, Almén and Tamelander, 2020] depending on its gestation period and other limiting aspects.

50 While some studies suggest that the peak timing of zooplankton may not change in parallel with
51 phytoplankton blooms [Winder and Schindler, 2004], others indicate that lag exists between primary
52 production and the transfer of energy to higher trophic levels [Brock and McClain, 1992, Brock et al.,
53 1991]. In their work, Aparna et al. [2022] (A22 from hereon) had shown that peak zooplankton
54 population may never occur even with a bloom in phytoplankton such as in SEAS, leading to the
55 collapse of ecological models and succeeding food webs of higher trophic levels.

56 The conventional zooplankton measurements, where only few snapshot/s of the event is captured
57 gives an incoherent or incomplete understanding in terms of spatio-temporal variation of zooplank-
58 ton [Ramamurthy, 1965, Piontkovski et al., 1995, Madhupratap et al., 1992, 1996a, Wishner et al.,
59 1998, Kidwai and Amjad, 2000, Barber et al., 2001, Khandagale et al., 2022] as much information
60 is revealed by later studies [Jyothibabu et al., 2010, Vijith et al., 2016, Shankar et al., 2019, Aparna
61 et al., 2022] using high resolution data. Calibrated acoustic instruments such as Acoustic Doppler

62 Current Profiler (ADCP) along with relevant data can be utilised to understand small scale vari-
63 ability [Nair et al., 1999, Edvardsen et al., 2003, Smith and Madhupratap, 2005, Smeti et al., 2015,
64 Kang et al., 2024], the complex interplay between the physico-chemical parameters and ecosystem
65 [Jiang et al., 2007, Potiris et al., 2018, Shankar et al., 2019, Aparna et al., 2022, Nie et al., 2023], the
66 zooplankton migration [Inoue et al., 2016, Ursella et al., 2018, 2021] and their seasonal to annual
67 variation [Jiang et al., 2007, Hobbs et al., 2021, Liu et al., 2022, Aparna et al., 2022].

68 1.2 ADCP backscatter and zooplankton biomass

69 At present, there are two types of acoustic samplers: non-calibrated single frequency acoustic profiler
70 such as ADCP or calibrated multi and mono frequency acoustic profilers such as zooplankton
71 acoustic profiler (ZAP) and Tracor acoustic profiling system(TAPS). The use of acoustics as a
72 proxy for zooplankton biomass estimation can be traced to Pieper [1971], Sameoto and Paulowich
73 [1977] and earlier studies which used echograms to approximate the large-scale horizontal extents
74 [Barraclough et al., 1969], and small scale vertical extent [McNaught, 1968]. The relationship
75 between backscatter and the abundance and size of zooplankton was described by Greenlaw [1979]
76 wherein it was pointed out that single frequency backscatter can be used to estimate abundance if
77 mean zooplankton size is known. This paved the way for use of single frequency acoustic profiler. A
78 drastic increase in study temporal and spatial variation of zooplankton biomass using backscatter-
79 proxy came in 1990s by introduction of high frequency echo sounders, with studies [Flagg and Smith,
80 1989, Wiebe et al., 1990, Batchelder et al., 1995, Greene et al., 1998, Rippeth and Simpson, 1998]
81 methodically showing acoustic backscatter estimated zooplankton biomass in various shelf and slope
82 locations around North Atlantic, North pacific location. The foundation for further research that
83 investigated the potential of acoustic backscatter from ADCPs and multi frequency echo sounders

84 in assessing zooplankton biomass and comprehending zooplankton dynamics in diverse maritime
85 habitats was established by these initial explorative experiments.

86 Acoustic backscatter and zooplankton biomass have been better understood as a result of tech-
87 nological and methodological developments over time. Net sampling augmented ADCP backscatter
88 have been used to study DVM and the spatial and temporal variability of zooplankton biomass in
89 different marine regions, such as the Southwestern Pacific, the Lazarev Sea in Antarctica and the
90 Corsica Channel in the north-western Mediterranean Sea [Cisewski et al., 2010, Hamilton et al.,
91 2013, Smeti et al., 2015, Guerra et al., 2019]. The zooplankton biomass variation in the Arabian
92 sea has been studied during JGOFS programme in 1990s [Herring et al., 1998, Nair et al., 1999,
93 Fielding et al., 2004, Smith and Madhupratap, 2005]. However, their studies were limited to the
94 cruise duration as vessel mounted ADCPs were predominantly used; hence long-term data was
95 sparsely produced. The first such study to fully exploit the immense potential of ADCPs in EAS
96 was carried out by A22 using ADCP moorings deployed on continental slopes off the Indian west
97 coasts [Amol et al., 2014, Chaudhuri et al., 2020].

98 1.3 Objective and scope of the manuscript

99 A network of ADCPs has been installed off the continental slope and shelf on the west coast of India.
100 This ADCPs have enabled a rigorous view of intraseasonal to seasonal scale variability [Amol et al.,
101 2014, Chaudhuri et al., 2020]. Initially a network of four ADCPs (off Mumbai, Goa, Kollam and
102 Kanyakumari) on continental slope, it has been extended to include three more moorings (off Okha
103 from 2018, Jaigarh and Udupi from 2017). In the recent study A22 have used ADCP moorings
104 off Mumbai, Goa and Kollam to explain the temporal variability of zooplankton biomass. The
105 study showed that the zooplankton peaks (and troughs) is not only non-uniform in latitude but

106 also heavily influenced by the oxygen minimum zone, MLD and the seasonal upwelling/downwelling
107 conditions. Stark contrast in the phytoplankton bloom and subsequence growth of zooplankton or
108 the lack thereof was observed in the EAS regimes.

109 We build upon the existing work by extending to include the newly incorporated ADCPs so as to
110 have a better understanding in the latitudinal variation of zooplankton biomass in EAS. The paper
111 is organized as follows; datasets and methods employed are described in detail in Section 2. Section
112 3 describes the observed climatology of zooplankton biomass and standing stock. A comparison is
113 drawn to the results of previous studies at the overlapping mooring sites. Further, the seasonal cycle
114 of zooplankton biomass and standing stock is discussed. The role of mixed layer depth, net primary
115 production, sea surface temperature, wind forcing and circulation in determining the biomass is
116 discussed in results section 4, with conclusion in section 5.

117 2 Data and methods

118 The backscatter data from ADCP and the zooplankton samples collected from the periphery of
119 mooring is described in this section. The methodology followed in processing ADCP data and
120 estimation of backscatter and subsequently the zooplankton biomass is discussed. The backscatter
121 derived from the echo intensity of the seven ADCP mooring deployed on the continental slope off
122 the Indian west coast is the primary data we have use in this manuscript. The moorings details are
123 summarized in [Table 1](#). In situ biomass data from volumetric zooplankton samples are used to val-
124 idate and correlate with backscatter. The chlorophyll data is obtained from marine.copernicus.eu.
125 In addition, we have used the monthly climatology of temperature and salinity [[Chatterjee et al.,](#)
126 [2012](#)] and the net primary productivity from MODIS (Moderate Resolution Imaging Spectrogra-
127 diometer) and VIIRS (Visible Infrared Imaging Radiometer Suite) from global NPP estimates

¹²⁸ (<http://sites.science.oregonstate.edu/ocean.productivity>).

¹²⁹ 2.1 ADCP data and Backscatter estimation

¹³⁰ The ADCPs were deployed on the continental slope off the Indian west coast ([Fig. 1](#)), off Mumbai,
¹³¹ Goa, Kollam and Kanyakumari, and later extended to three more sites to cover the entire EAS
¹³² basin from Okha (22.26°N) in north to Kanyakumari (6.96°N) in south. The other two ADCPs
¹³³ are Jaigarh at central EAS (CEAS) and Udupi in the transition zone between CEAS & SEAS. The
¹³⁴ extended moorings were deployed in October 2017, except for Kanyakumari which was deployed
¹³⁵ earlier as well but it wasn't part of the earlier backscatter study by A22. The moorings are serviced
¹³⁶ on yearly basis usually during October-November or in winter monsoon months. The ADCPs are
¹³⁷ of RD Instruments make, upward-looking and operate at 153.3 kHz. While utmost care is taken to
¹³⁸ position the instrument at ~ 200 m depth, yet for some deployments it's shallow or deeper owing
¹³⁹ to drift caused by floater buoyancy - anchor weight balance. Data was collected at hourly interval
¹⁴⁰ and the bin size was set to 4 m. The echoes at surface to 10 % range (~ 20 m) means the data at
¹⁴¹ these depths is rendered useless and is discarded from further use.

¹⁴² The procedure followed in processing of the ADCP data are described in [Amol et al. \[2014\]](#) and
¹⁴³ [Mukherjee et al. \[2014\]](#). Depth correction was an addition to their methodology to accommodate
¹⁴⁴ the vertical movement of ADCP buoys [[Chaudhuri et al., 2020](#), [Mukhopadhyay et al., 2020](#)] using
¹⁴⁵ data from pressure sensor mounted on the instrument. We have followed the methodology laid down
¹⁴⁶ in A22 to derive the backscatter time series from ADCP echo intensity data which is discussed later
¹⁴⁷ paragraph. The gaps up to two days are filled using the grafting method of [Mukhopadhyay et al.](#)
¹⁴⁸ [[2020](#)] once the zooplankton biomass time series is constructed.

¹⁴⁹ The primary objective of ADCP usage is to obtain vertical current profile at a point location.

150 It is achieved by using the echo intensity received at the ADCP transducer. The instrument
151 sensors doesn't directly give backscatter, as echo intensity is range independent. Range correction
152 has to be performed before echo intensity (E) is converted to Backscatter (B). Received signal
153 strength indicator (RSSI), also called the conversion factor (K_c) is sensor specific and is used with
154 the corresponding reference echo intensity (E_r). It's important to state that for the same device
155 K_c remains unchanged while E_r may vary over each subsequent deployment. The backscattering
156 strength (in dB) is given by [Mullison \[2017\]](#):

$$157 \quad B = [C - L_{DBM} - P_{DBW}] + 2\alpha R + 10\log_{10}[(T_{TD} + 273.16)R^2] + 10\log_{10}[10^{K_c(E-E_r)/10} - 1]$$

158 where C is an empirical constant, L_{DBM} is $10\log_{10}L$ where L is the transmit pulse length in
159 meters, P_{DBW} is $10\log_{10}P$ (P is transmitted power in watts), α is the sound absorption coefficient
160 of water (in $dB m^{-1}$), T_{TD} is the temperature (in ${}^\circ C$) at the depth of positioned instrument, R
161 is the slant range (in meters) from transducer to the scatterers and E_r is the reference level of E
162 taken in real-time (unit counts). E_r in our case is taken from first (last) measured profile when the
163 instrument is in air before (after) deployment (retrieval). The backscattering strength is referenced
164 to $(4\pi m^{-1})$ [[Deines, 1999](#), [Mullison, 2017](#)]. A22 has discussed the relevance of each of the term to
165 the total backscattering strength. Our analysis also suggests that the α does not affect the final
166 results.

167 2.2 Zooplankton data and estimation of biomass

168 The zooplankton samples were collected in the vicinity (~ 10 km) of ADCP mooring site twice; once
169 prior retrieval and again post deployment of moorings so that there is overlap in the ADCP time
170 instance and in situ zooplankton samples. The sampling is done at the mooring location during
171 servicing cruises on board RV Sindhu Sankalp and RV Sindhu Sadhana (Table 2). Multi-plankton

¹⁷² net (MPN) (100 μm mesh size, 0.5 m^2 mouth area) was used to get samples in the pre-determined
¹⁷³ depth ranges; water volume filtered was calculated by the product of sampling depth range and the
¹⁷⁴ mouth area of net. The depth range and timing of sample collection was different throughout the
¹⁷⁵ MPN hauls (refer [Table 2](#)). From 2020 onward, the depth-range was standardized to the bins of 0
¹⁷⁶ - 25, 25 - 50, 50 - 75, 75 - 100, 100 - 150 (units are in meters). The collected zooplankton samples
¹⁷⁷ were then preserved in 5 % formaldehyde solution until it's transferred to laboratory. To measure
¹⁷⁸ zooplankton wet weight accurately, the gelatinous forms/salps were separated. A22 had reported
¹⁷⁹ the calanoid copepods, cyclopoid copepods, Poecilostomatoida, Harpacticoida, appendicularians,
¹⁸⁰ euphausiids, ostracods, and chaetognaths as the major groups of zooplanktons contributing to the
¹⁸¹ biomass of net samples from the mooring sites. The backscatter obtained earlier is averaged in
¹⁸² vertical corresponding to the specific MPN hauls for each site. The backscatter is linear regressed
¹⁸³ with respective biomass to establish their relationship, which has been demonstrated in numerous
¹⁸⁴ previous studies [[Flagg and Smith, 1989](#), [Heywood et al., 1991](#), [Jiang et al., 2007](#), [Aparna et al.,](#)
¹⁸⁵ [2022](#)].

¹⁸⁶ We calculated the regression equation to be $y = 0.0203 x + 4.01$ and, which is well within the
¹⁸⁷ error range of the regression equation of A22, $y = (0.02 \pm 0.004) x + (4.14 \pm 0.36)$ with a correlation
¹⁸⁸ of 0.53 ([Fig. 2](#)). The correlation value in our case is 0.54; the minor difference is due to higher
¹⁸⁹ number of data points (159) in the present study.

¹⁹⁰ **2.3 Biomass time series and estimation of standing stock**

¹⁹¹ The zooplankton biomass time series ([Fig. 3](#)) is created from the above derived linear relationship:
¹⁹² $\log_{10}(\text{biomass}) = m * \text{Backscatter} + k$, where m is slope and k is intercept. The time series shows
¹⁹³ the pattern of diel vertical migration (DVM) at all the mooring sites during dawn (\sim 0600-0700)

hours) and dusk (\sim 1800-1900 hours). It is evident in earlier studies using backscatter [Ashjian et al., 2002, Smith and Madhupratap, 2005, Inoue et al., 2016, Ursella et al., 2018] and in situ zooplankton data [Padmavati et al., 1998]. The implication of DVM is a higher biomass at surface during the night as zooplankton feeds and a lower biomass at daytime as they descend to subsurface depths. The overall biomass over the time period of a day may vary but the DVM doesn't affect the seasonal variation as shown by Jiang et al. [2007] and A22. Since our goal is to study the seasonal variation, delineating the daily biomass is sufficient. The biomass time series and it's seasonal cycle is discussed in subsection 4.1.

The standing stock is determined by taking the depth integral of biomass over the water column. To maintain the consistency of standing stock estimation, only those deployments that doesn't lack data at any depth in the entire range of 24 - 120 m are considered for analysis. The lack of data in the above mentioned depth range is due to deviation in positioning of ADCP sensor in the water column. A swift alteration in bathymetry along the continental slope implies that the mooring might anchor at a different depth than planned, hence a change in the predicted position of ADCP. This leads to gap in data at few mooring sites for some year. For example, for the northern-most mooring at Okha, data is not available for the entire upper 120 m depth for the second deployment. Also at Jaigarh, where the surface to \sim 60m data (in 3rd deployment) and Kollam, where 80 m and below (in 4th deployment) is unavailable and hence discarded from standing stock estimation. There are few deployments where no data or bad data was recorded e.g, at Udupi (4th deployment) and Kanyakumari (6th deployment). The seasonal cycle of standing stock for 24 - 120 m available data is explored in subsection 4.2.

Through the findings of biomass variability in different time scale, we hypothesize that current may influence the zooplankton biomass by driving nutrients and phytoplankton rich water. Wavelet

217 coherence between current and biomass is taken for each depth, and from this data, the coherence
218 and phase at annual period is taken to check for dependency of biomass on current. In [subsection 4.3](#)
219 we shed a light on possible dependency of biomass on zonal & meridional current.

220 2.4 Mixed-layer depth, temperature and oxygen

221 As we are using a 153.3 kHz ADCP moored at \sim 150 m, the top \sim 10% of data is unusable because
222 of surface echoes. MLD in EAS is of the order \sim 20 to 40 m during summer monsoon [[Shetye](#)
223 [et al., 1990](#), [Sreenivas et al., 2008](#)] especially in the SEAS, but during winter the MLD in northern
224 NEAS remains deep [[Shankar et al., 2016](#)]. Although it is possible to use the near surface ADCP
225 data after due noise correction; it is beyond the scope of present study. The temperature data is
226 used from [Chatterjee et al. \[2012\]](#), a monthly climatology having 1° spatial resolution. Monthly
227 climatology of oxygen data is obtained from World Ocean Atlas 2013 [[García et al., 2014](#)] which
228 contains objectively analyzed 1° climatological fields of in situ measurements.

229 2.5 Chlorophyll and net primary productivity data

230 Previous study based on ADCP data of EAS A22 have used SeaWiFS based chlorophyll data for
231 comparison with climatology of zooplankton standing stock (ZSS). The SeaWiFS was at its end
232 of service in 2010, hence we use new chlorophyll product. The present study has been conducted
233 using Global Ocean Colour, biogeochemical, L3 data obtained from the [E.U. Copernicus Marine](#)
234 [Service Information](#). The daily data is available at a spatial resolution of 4 km.

235 While chlorophyll is used to compare with the variation in climatology of zooplankton standing;
236 the growth efficiencies of zooplankton are directly linked to primary production levels, emphasizing
237 the interconnectedness between primary producers and consumers in marine food webs [[Friedland](#)

²³⁸ et al., 2012]. In their study, A22 has emphasized on the collapse of the predator-prey relationship
²³⁹ between zooplankton-phytoplankton using climatological data. We showcase their interdependency
²⁴⁰ or the lack thereof using net primary productivity models. Moderate Resolution Imaging Spectro-
²⁴¹ radiometer (MODIS) based net primary productivity (NPP) data at a resolution of $0.16^{\circ} \times 0.16^{\circ}$
²⁴² was obtained from Oregon State University. They have employed three different schemes to obtain
²⁴³ NPP from Chlorophyll concentration. Those are discussed below in brief. The first is Vertically
²⁴⁴ Generalized Production Model (VGPM). The NPP (a rate term) is to be derived from chlorophyll
²⁴⁵ (a standing stock) using chlorophyll-specific assimilation efficiency for carbon fixation. The single
²⁴⁶ biggest unknown in all models based on chlorophyll is how this rate term is described. VGPM
²⁴⁷ considers the primary productivity to be dependent on day length and maximum daily NPP within
²⁴⁸ a water column. The second is Carbon-based Productivity Model (CbPM) which NPP to phy-
²⁴⁹toplankton carbon biomass and growth rate. The third is Carbon, Absorption, and Fluorescence
²⁵⁰ Euphotic-resolving (CAFE) mode; first described in Silsbe et al. [2016] takes various other factors
²⁵¹ into NPP calculations. We explore these NPP models and try to explain the variation in ZSS.

²⁵² 3 Climatology of zooplankton biomass and standing stock

²⁵³ The previous study of zooplankton in EAS based on ADCP backscatter was consisting of three
²⁵⁴ sites: Mumbai in NEAS, Goa in CEAS and Kollam in SEAS. The extended mooring sites are at
²⁵⁵ Okha at NEAS, Jaigarh at CEAS, Udupi in the transition zone of CEAS & SEAS and Kanyakumari
²⁵⁶ at SEAS is the southern most location in our study area.

²⁵⁷ ADCP data from three mooring sites were analysed from 2012 to 2020 in A22. They have
²⁵⁸ fine-tuned the methodology to obtain backscatter and estimated zooplankton biomass from it using
²⁵⁹ in situ volumetric zooplankton biomass data. A comparison is made in later paragraphs, since the

260 methodology remains same in the current study and new time series data is available. The monthly
261 climatology of biomass and ZSS is computed for all locations having valid data in 24 - 140 m depth
262 range ([Fig. 4](#)).

263 The high biomass regime in the upper ocean and low biomass regime in deeper depths is differ-
264 entiated using a biomass contour: 215 mg m^{-3} off Mumbai, Goa, Kollam, Jaigarh and Udupi; 175 mg m^{-3} off Okha and Kanyakumari. For simplicity, this biomass contour is abbreviated to be z215
265 & z175 and its depth is denoted as D215 & D175, respectively. The choice of biomass contour isn't
266 abrupt; firstly, it is carefully chosen to accommodate the seasonal variation, as a shift to biomass
267 contour lower than the z215 would be unviable as our data is only till 140 m depth, for example in
268 the case of Kollam, the D215 exceeds 140 during few months of 2022 ([Fig. 3](#)). A higher biomass
269 contour would lead to inferior view of the seasonal cycle as in the case of Kanyakumari and Okha
270 where 215 mg m^{-3} biomass contour is often low enough to reach $\sim 20 - 30 \text{ m}$ depths, hence z175 is
271 chosen here. Secondly, it allows us to link the seasonal variation of biomass to the physico-chemical
272 properties.

274 The climatology of zooplankton biomass and ZSS ([Fig. 4](#)) is discussed at locations northward
275 starting from southernmost mooring site off Kanyakumari.

276 3.1 Southern EAS

277 During mid-march off Kanyakumari, the depth of 23° C isotherm (henceforth D23) shallows along-
278 with oxycline (marked by 2.1 ml L^{-1}) and a rise in biomass is observed ([Fig. 4 g1](#)). The z175
279 is shallower from May onward to October and the zooplankton biomass is comparatively higher
280 than rest of the year. The D175 deepens starting from October and the relatively high biomass in
281 water column is maintained till late December. However, this increase in D175 isn't reflected as

²⁸² an increase in ZSS because of low biomass in the entire water column. A gradual increase is seen
²⁸³ in the chlorophyll biomass starting from April and the peak is attained in June ([Fig. 4 g2](#)). The
²⁸⁴ ZSS is increased in June, however the growth is minimal. There is almost no seasonal variation
²⁸⁵ in ZSS off Kanyakumari (seasonal ZSS range, 2.67 gm m^{-2}) as compared to the ZSS variation at
²⁸⁶ the nearest northern mooring site off Kollam (seasonal ZSS range, 4.86 gm m^{-2}), where a strong
²⁸⁷ seasonal cycle is observed and the D215 is deeper for any given month.

²⁸⁸ Off Kollam, a higher biomass is present in the larger portion of water column and the D215 is at
²⁸⁹ $\sim 110 \text{ m}$ during Mar-May ([Fig. 4 f1](#)). Similar to z175 off Kanyakumari, the decrease in biomass with
²⁹⁰ depth is subtle below z215. Starting from March, the D215 begins to shallow with progress in time
²⁹¹ till August. During this period, a sharp decrease is seen in the D23 ($\sim 80 \text{ m}$ in June to September)
²⁹² while the oxycline (1.7 ml L^{-1}) overshoots the thermocline ([Fig. 4 f1](#)). A steep rise in chlorophyll
²⁹³ biomass is seen off Kollam and its peak is attained in August ([Fig. 4 f2](#)). The ZSS declines in the
²⁹⁴ same period and reaches a minimum when the chlorophyll biomass is at its peak. The chlorophyll
²⁹⁵ biomass decreases rapidly in the following months, while the ZSS increases and a maximum is seen
²⁹⁶ during October. This feature was earlier reported by A22 showing disproportionate interaction
²⁹⁷ between zooplankton and phytoplankton. It begs the question about existing understanding of
²⁹⁸ predator - prey relationship in a regional-scale ecological system. A similar feature is seen further
²⁹⁹ north, off Udupi which sits at the transition zone of SEAS & CEAS, albeit with a relatively weaker
³⁰⁰ zooplankton biomass. The peak of chlorophyll and minimum of ZSS occurs in September ([Fig. 4 e2](#))
³⁰¹ which is one month later than off Kollam. The 2.1 ml L^{-1} oxygen contour overshoots thermocline,
³⁰² however it reaches to a much shallow depth of $\sim 20 \text{ m}$ during July to October unlike any other
³⁰³ location in our EAS study area. The D215 vaguely follows D23; with the gradual shallowing from
³⁰⁴ March onward reaching $\sim 60 \text{ m}$ in September and a steep decline afterwards till November ([Fig. 4](#)

305 e1). The decrease of biomass with depth is moderate in comparison to Kollam.

306 **3.2 Central EAS**

307 Off Goa, the D215 seasonal trend is similar to Udupi and is entirely restricted by D23 & 1.7 ml L^{-1}
308 oxygen contour that closely follows it. During March-May, the D215 is at $\sim 80 - 100 \text{ m}$ which
309 shallows with onset of summer monsoon ([Fig. 4 d1](#)); the chlorophyll biomass increases during this
310 period and the maximum occurs in August after which the chlorophyll biomass and ZSS ([Fig. 5](#))
311 both decrease in September. Although we witness an increase in chlorophyll biomass in October,
312 the D215 is restricted to the $\sim 50 \text{ m}$ in this period and the ZSS is at its minimum similar to what
313 is observed off Udupi (Kollam) during September (August). The ZSS rapidly increases and reaches
314 its maximum in January, sustained till March and then gradually declines. Unlike the previous
315 locations, the biomass off Goa decreases rapidly below the z215 as reported earlier in A22, reaching
316 as low as 60 mg m^{-3} at 130 m during June to September ([Fig. 4 d1](#)).

317 The ZSS off Jaigarh is identical but stronger to that of off Goa, owing to an higher biomass above
318 z215 and the comparatively deeper D215 ([Fig. 4 c1](#)). The D215 follows D23 & oxycline for most
319 of the year and it only exceeds during October-December. From the ZSS maximum in February
320 ([Fig. 4 c2](#)), it steadily decreases and attains a minimum in September (coincides with lower D200),
321 a rapid rise is seen in the following months. What's intriguing is a presence of strong seasonal cycle
322 in ZSS off Jaigarh (10.38 gm m^{-2} , highest among all locations) although the seasonal variation in
323 chlorophyll biomass ([Fig. 4 c2](#)) is visibly non-existent (0.15 mg m^{-3} , lowest among all locations).
324 This is an exact opposite scenario of Kanyakumari site, where an insignificant seasonal variation in
325 ZSS (2.67 gm m^{-2}) is seen even though the chlorophyll biomass varies strongly (1.62 mg m^{-3}).

326 Starting from Kollam ([Fig. 4 f1](#)) and moving northward to Jaigarh ([Fig. 4 c1](#)), we see that the

³²⁷ core of high zooplankton biomass gradually shifts from summer monsoon (off Kollam) to winter
³²⁸ monsoon (off Jaigarh), with the transition of upper ocean zooplankton biomass happening along
³²⁹ Udupi and Goa. On the contrary, the chlorophyll biomass tends to have low seasonal range as we
³³⁰ move northward from SEAS, with Jaigarh having the least seasonal variation.

³³¹ **3.3 Northern EAS**

³³² Further north of Jaigarh, off Mumbai the D215 follows a similar pattern i.e, a deeper D215 in
³³³ December to early April, resulting in a higher ZSS in the same period ([Fig. 4 b2](#)). The D23 off
³³⁴ Mumbai follows D215 and the oxycline follows an erratic pattern, reaching depths > 140 during
³³⁵ January to March ([Fig. 4 b1](#)); when a higher biomass is observed above z215. The chlorophyll
³³⁶ biomass shows seasonal variation albeit lower than the SEAS counterpart. Its peak occurs in
³³⁷ August, then decreases rapidly and increases from October onward maintaining the biomass at 0.5
³³⁸ $mg\ m^{-3}$ till March. In zooplankton biomass climatology, during September-October a thin layer
³³⁹ of low biomass regime is seen at depths ~30 - 40 m, combined with shallow D215 resulting in a
³⁴⁰ ZSS minimum. The ZSS increases rapidly from its minima in October in the following month as
³⁴¹ the D215 deepens and the maximum occurs in February. The chlorophyll biomass decreases from
³⁴² March and a gradual decrease in ZSS is seen till July, after which the ZSS basically flattens even
³⁴³ though the chlorophyll increases.

³⁴⁴ At the northernmost site of EAS i.e, off Okha, a noticeable feature is a much higher oxygen in
³⁴⁵ upper ocean except during summer monsoon. The biomass above z200 is much weaker ([Fig. 4 a1](#))
³⁴⁶ compared to Mumbai as seen in the zooplankton biomass climatology which leads to a relatively
³⁴⁷ lower ZSS ([Fig. 4 a2](#)). The D200 shallows from February (coinciding with ZSS maximum) to its
³⁴⁸ minimum in August, remains visibly flat till September and then increases steadily till December

349 and rapidly afterwards. There's two chlorophyll peak off Okha; one in February [Keerthi et al.,
350 2017] and the other during August in summer monsoon [Lévy et al., 2007]. The ZSS remains flat
351 in summer monsoon period i.e, June to September, although the chlorophyll biomass increases in
352 this time. Afterwards, ZSS gradually increases and attains its maximum in February same as the
353 chlorophyll biomass. The ZSS sustains this maximum till March, declines rapidly in April and then
354 gradually till July.

355 3.4 Comparison to previous result

356 A comparison with the zooplankton biomass and standing stock climatology of previous work A22
357 is made in this section for the locations of Mumbai, Goa and Kollam. In the previous study data
358 from 2012 to 2020 is used, while the present study includes data from 2017 to 2023.

359 It is observed that D215 is shallower at all locations and as a result a lower ZSS is seen in the
360 climatology of the present study (Fig. 5). The difference in D215 is prominent off Goa; while in the
361 previous climatology (Fig. 5 b1) the D215 is deeper and lies along D23, in the present climatological
362 data (Fig. 5 b2) the D215 is shallower and lies \sim 20 - 40 m above the D23 during January to April.

363 A relatively lower biomass is present above z215 year round which reflects in overall lower ZSS. This
364 goes same for the biomass off Mumbai (Fig. 5 a1 & a2) i.e, a comparatively shallow D215 and lower
365 ZSS in comparison with [Aparna et al., 2022]. Instead of a ZSS maxima in February, in the present
366 data, the maxima is sustained in march, which could be due to the lower value of ZSS in February.
367 The second maxima occurs in August (Fig. 5 d1) which is less pronounced in present study (Fig. 5
368 d2). Similar to Goa, there is dramatic decrease in the minima that occurs in October and ZSS
369 increases rapidly post October till February. Off Kollam, a higher biomass is observed from May to
370 June in previous study, while in the present study, along with May to June, a higher biomass is seen

371 from September to November([Fig. 4 c2](#)) which is reflected as a minima of ZSS occurring in August
372 ([Fig. 4 d2](#)). The higher ZSS on either side to this minima is less pronounced in previous data. This
373 difference in ZSS is clearly seen in the correlation, which is 0.60 off Kollam, while it is 0.94 and 0.98
374 off Mumbai and Goa, respectively. Note that the correlation only shows how similar the ZSS trend
375 is and doesn't tell us about the deviation in magnitude in present study. Chlorophyll biomass shows
376 stronger peak for all locations in August in present study, when the zooplankton-phytoplankton
377 relationship discrepancy is observed off Kollam similar to results reported in previous climatology.

378 4 The seasonal cycle and variability

379 In the following section we will describe the zooplankton biomass time series followed by a discussion
380 on the seasonal cycle.

381 Biomass contour to demarcate upper (high biomass) to lower (low biomass) regimes is devised
382 for each zooplankton time series to show their seasonality. A preliminary analysis of the biomass
383 time series in daily and monthly averaged scale shows that the biomass decreases with increasing
384 depth ([Fig. 3](#)) at all the seven locations. The rate of biomass decrease with depth, roughly defined
385 as the difference between the mean biomass at 40 m and 104 m depth, is highest off Jaigarh and
386 Mumbai as it has higher biomass in upper ocean ([Fig. 6 c,b](#)). This is followed by CEAS locations
387 Goa and Udupi ([Fig. 6 d,e](#)). While the biomass decrease with depth is lower off Kollam from
388 2017 to 2020, it becomes considerably high from thereon ([Fig. 6 f](#)). The rate of decrease is lowest
389 off Kanyakumari. Following is the order of their decrease rate of biomass: Jaigarh (96 mg m^{-3}),
390 Mumbai (91 mg m^{-3}), Okha (79 mg m^{-3}), Udupi (78 mg m^{-3}), Kollam(73 mg m^{-3}), Goa (72 mg m^{-3}) and Kanyakumari (39 mg m^{-3}). The mean and standard deviation is shown in [Table 3](#).
392 Following poleward along the slope, the mean biomass at 40 m off Kanyakumari is the least ~

207 $mg\ m^{-3}$ which increases drastically to 272 $mg\ m^{-3}$ off Kollam. It decreases till Goa and then increases to a maximum of 278 $mg\ m^{-3}$ off Jaigarh. Off Mumbai the mean biomass is 272 $mg\ m^{-3}$, and further north off Okha, it declines to 230 $mg\ m^{-3}$. A similar trend is observed in mean biomass at 104 m depth of all locations and their corresponding standard deviation. A pattern that develops from this is observed, with lower mean biomass off Okha (northernmost of EAS) and off Goa (CEAS) bifurcated by higher mean biomass off Mumbai & Jaigarh; while the lower mean biomass off Udupi (CEAS) and off Kanyakumari (Southernmost of EAS) is divided by higher mean biomass off Kollam. Similarly, from standard deviation of biomass it is inferred that the sites with higher biomass tends to have higher variation over time as in the case of Mumbai, Jaigarh and Kollam.

A comparatively weaker decline in zooplankton biomass with respect to depth off Okha ([Fig. 3 a1,a2](#)) at NEAS is agreeing with earlier reported data [Madhupratap et al. \[2001\]](#), [Smith and Madhupratap \[2005\]](#), [Wishner et al. \[1998\]](#) where oxygen deficit is thought to be the cause, particularly during summer monsoon seen in [García et al. \[2014\]](#) climatology (figure not shown). The sites at SEAS, especially off Kanyakumari and 2017 to 2020 off Kollam also have weaker decrease [[Madhupratap et al., 2001](#), [Aparna et al., 2022](#)]. However, post 2020 the decline in biomass with depth off Kollam is similar to that off Mumbai in stark contrast to its previous years owing to a strong bloom in these years. This growth is reflected as an increase in biomass in the entire water column ([Fig. 3 f1,f2](#)) and deepening of D215. Analyzing the demarcating biomass contours (z175, z215 of respective locations) we see a strong seasonality at NEAS, CEAS and SEAS (excluding Kanyakumari). Although a shallow and seasonally invariant D215 is seen for Goa and Kollam during January 2019 to December 2020. While the z175 and z215 is deeper in winter monsoon throughout EAS, at the NEAS regime, the upper ocean shows considerably high biomass during this period as in the case

416 of Okha, Mumbai and Jaigarh. On the contrary, at SEAS regime the upper ocean shows higher
417 biomass during summer monsoon as seen off Udupi, Kollam and Kanyakumari even though the
418 z215 & z175 is shallower in this period.

419 **4.1 Seasonal cycle of biomass**

420 Although the variation in zooplankton biomass time series is inferred from the standard deviation
421 at 40 & 104 m depth, it provides no information about the seasonal cycle. The evaluation is made
422 from performing wavelet analysis on the time series. In the investigation of dominant periods, it is
423 valid to compare the wavelet power (or variability) along a particular period across the time series,
424 but a cross-period wavelet power comparison is not possible [Maraun and Kurths, 2004, Chaudhuri
425 et al., 2020]. It is due to the normalization process which stresses more on the wavelet power of
426 higher period, and hence for the same wavelet power a lower period would have higher variability
427 compared to a higher period.

428 **4.1.1 The annual cycle**

429 The time series has loss of data due to instrument fault or improper position of ADCP in the
430 water column. For example, off Okha during it occurred in the second deployment (Dec-2019 to
431 Dec-2020), the instrument was way below from it's intended depth of 150 m leading to no data in
432 top 140 m water column. It is not possible to construct a continuous record and hence it makes
433 it difficult to interpret the annual cycle where ever the data record is short. So, for 40 m biomass
434 time series we restrict our description to all locations except Okha and Jaigarh while performing
435 wavelet analysis.

436 Off Mumbai, a strong annual cycle (~ 365 days) dominates the seasonal cycle throughout the

437 time series ([Fig. 7 b](#)). Annual cycle is comparatively weak off Goa (CEAS) contrary to results of
438 A22 which could be due to shorter time record and low biomass in the recent years. The annual
439 cycle off Udupi & Kollam (SEAS) is strong, however it varies in time and off Kollam the wavelet
440 power is stronger post 2020 ([Fig. 7 f](#)). Further south, off Kanyakumari, the annual cycle weakens
441 having power similar to that of Goa.

442 At 104 m, the annual cycle strengthens off Mumbai and Goa ([Fig. 8 b, d](#)) compared to the
443 annual cycle at 40 m; implying that the biomass seasonal variation at 104 m is robust even though
444 the mean biomass is considerably lower. Annual cycle weakens off Kollam ([Fig. 8 f](#)), although only
445 vague interpretation can be made as it lies beyond the cone of influence.

446 4.1.2 The semi-annual cycle

447 Along with the annual cycle, we observe presence of semi-annual (~ 180 days) cycle at most locations
448 and together they constitute the seasonal cycle. At 40m depth Off Okha the semi-annual period is
449 weak. Off Mumbai however, the semi-annual cycle is present throughout the record and becomes
450 stronger in 2022-2023 ([Fig. 7 b](#)) but not as much as the annual cycle. At Goa we see that the
451 semi-annual period dominates seasonal cycle in the same duration ([Fig. 7 d](#)). The dominance
452 of semi-annual cycle is also seen off Kollam. Although the dominance of semi-annual period in
453 seasonal cycle is seen only for some years, a similar feature was discussed for WICC where the
454 intra-annual component dominates the seasonal cycle as we go equatorward with a change in the
455 strength of intra-annual component in time [[Chaudhuri et al., 2020](#)]. However, off Kanyakumari
456 the semi-annual cycle is absent ([Fig. 7 g](#)).

457 Unlike the annual band which becomes stronger at 104 m, the semi-annual band weakens off
458 Mumbai & Goa at the same depth ([Fig. 8 b,d](#)). While the semi-annual band at 104 m becomes

459 relatively stronger compared to the semi-annual band at 40 m off Okha ([Fig. 8 a](#)), it is almost
460 non-existent off Kanyakumari ([Fig. 8 g](#)). The wavelet power of semi-annual cycle is same at 40 m &
461 104 m off Mumbai, Goa and Kollam for most of the data record, but weakens at 104 m compared to
462 40 m during 2022. Investigating the longer time series off Mumbai, Goa and Kollam, it is observed
463 that the semi-annual cycle is comparable to the annual cycle at some instances such as in 2022 and
464 the its strength increases as we move equatorward.

465 **4.2 Seasonal cycle of standing stock**

466 The zooplankton standing stock time series is obtained by integrating the biomass over 24 - 120 m
467 of water column, ([Fig. 9](#)). The presence of significant variation in the 30-day running mean with
468 recurring burst is seen in the daily data. In NEAS regime, the ZSS maximum occurs during January
469 to late March and early April as seen off Okha, Mumbai, Jaigarh and Goa. However, the decline of
470 ZSS post the maxima is comparatively gradual off Goa which was also visible in the climatology of
471 ZSS ([Fig. 4 d2](#)). The growth in ZSS at NEAS sites during summer monsoon is much lower compared
472 to the SEAS. For example, off Kollam, we observe the presence of double peak, one during May to
473 July and the another during September to November. Similar feature is seen off Udupi, the nearest
474 northern site of Kollam, but with a much higher ZSS during September to November as compared
475 with May to July ZSS. Off Kanyakumari, although there seems to be intra-annual variations, a clear
476 annual cycle is not observed.

477 **4.2.1 The annual cycle**

478 The absence of annual cycle off Kanyakumari is confirmed with wavelet analysis ([Fig. 9 g1](#)). Off
479 Kollam, the presence of a weak annual cycle is seen contrary to a strong annual cycle of Udupi,

480 however a longer data record is needed as the annual period lies beyond the cone of influence. Off
481 Goa ([Fig. 9 d1](#)), the annual cycle was weak for 2018 to early 2020, which strengthened afterwards.
482 The annual cycle is strongest off Mumbai ([Fig. 9 b1](#)) throughout the data record and the wavelet
483 power is highest among all locations. Fourier analysis reveals the presence of strong annual cycle
484 off Jaigarh and Okha.

485 4.2.2 The semi-annual cycle

486 Although we observed the absence of annual cycle off Kanyakumari, the wavelet analysis shows
487 presence of a semi-annual cycle from early 2019 to late 2021([Fig. 9 g1](#)). This semi-annual feature is
488 seen off Kollam ([Fig. 9 f1](#)) with moderate power and with a much higher power off Udupi ([Fig. 9 21](#))
489 during 2018 to 2020. Much like the annual cycle off Goa, it's semi-annual period is weak to nearly
490 non existent before 2020 and gets strengthened afterwards. Off Mumbai, the semiannual period
491 is present from late 2018 to late 2020 and from 2022 onward. Fourier analysis shows that the
492 semi-annual cycle off Udupi is comparable to its counterpart off Mumbai during the same period.

493 The higher beta (β) coefficients off Jaigarh and Kollam implies a significant contribution of
494 low frequency variability (higher period) is more compared to the high frequency variability and is
495 discussed in detail in later section. In fact, a biennial peak is seen off Kollam in the Fourier analysis
496 even with a 3 year record agreeing with earlier findings of A22, i.e, Kollam having a weak (strong)
497 annual (biennial) cycle.

498 4.3 Annual, intra-annual and intraseasonal variability

499 The biomass at a given instance is decomposed to several exclusive period bands spanning days to
500 months. DVM is the simplest variation (low period or high frequency) among many that determines

501 zooplankton biomass at a given depth, with higher (lower) biomass during night (day) at the surface
502 regime for a number of species. Our focus, however is on the variability occurring in the higher
503 period (lower frequency) bands namely, annual, intra-annual and intraseasonal variability.

504 The strength and contribution of distinct components of variability differs in time and between
505 different regimes of EAS. For example, during 2019 off Kollam at 40 m depth, the variability in
506 shorter time scale (days to weeks) is dominated by high frequency components (< 30 days) ([Fig. 10](#)).
507 The contribution of high frequency components to the total biomass was evident in the beta value
508 in Fourier analysis, larger beta value implying a bigger contribution of the high frequencies than
509 the lower ones. An increase in biomass during summer monsoon of 2019 is facilitated by the low
510 frequency variability. However, during August a sharp decline in biomass is observed and the
511 decomposition of variability suggests that it is due to a decrease in intra-annual and intra-seasonal
512 variability even though the annual variability was weakly positive.

513 To capture the annual variability, the biomass is filtered with lanczos filter within period of 300 to
514 400 days. The annual variability shows that the contribution of this band to the time series of total
515 biomass is very weak. The annual variability off Kanyakumari (standard deviation 3.64 mg m^{-3})
516 and Okha (3.73 mg m^{-3}) is low, while it is stronger at rest of the basin, with strongest variability
517 off Jaigarh (9.05 mg m^{-3}). Similar to the ocean currents [[Amol et al., 2014](#), [Chaudhuri et al., 2020](#)],
518 the annual filtered biomass decreases strongly with depth off Kollam than off Mumbai and the three
519 CEAS sites ([Fig. 11](#)). Upward phase propagation in zonal and meridional current is observed at
520 almost all mooring sites and also seen in the annual filtered biomass time series, i.e, off Goa and
521 it's southern mooring sites. Owing to the above, advection as a driver to upwelling and further as
522 one of the cause for zooplankton growth is hypothesized and their relationship is explored. Wavelet
523 coherence shows that the current and biomass have strong coherence off Kanyakumari (2019,2021),

524 Kollam (2019, 2022) during May to late summer monsoon of 2019 with meridional current leading
525 biomass, when the currents are reversing with monsoon ([Fig. 12](#)). As we go poleward along the
526 slope, coherence exists but at different depth i.e, off Goa for 2019, the maximum coherence of
527 meridional current with biomass is at 50 to 80 m and again below 110 m. The feature observed
528 in annual filtered biomass off Goa is same as the alongshore component [[Nethery and Shankar,](#)
529 [2007](#)], with the core of biomass and alongshore current lying at about 50 m. Further north, off
530 Mumbai a shift in time of maximum coherence is observed occurring in winter monsoon at 80 m
531 and below with zonal current leading biomass. During pre-summer monsoon upwelling sets as early
532 as February in SEAS but only in May farther north along the coast [[Banse, 1968](#), [?](#)] which results
533 in shift in biomass coherence as we go poleward. Off Okha however, present of coherence is seen
534 throughout 2021 from 20 to 150 m with meridional current leading biomass which could be due
535 to a deeper MLD in northern NEAS [[Marra and Barber, 2005](#), [Shankar et al., 2016](#)]. This has
536 implications on the nature of zooplankton and fisheries found in regimes of EAS as we'll discuss.

537 The variability at intra-annual (100 - 250 days) band tends to be stronger compared to the an-
538 nual variability and is strengthened during late summer monsoon to transitional monsoon months
539 ([Fig. 13](#)) as seen during 2018, 2019 and 2022. Intra-annual variability of biomass increases equa-
540 torward with higher variation seen off Goa, Udupi and Kollam; although off Kanyakumari the
541 variability is reduced. However, Fourier analysis of the daily biomass time series suggests presence
542 of signals within the intra-annual band off Kanyakumari, e.g, power peaks at ~ 140 and ~ 220 days
543 implying that the variability is strictly restricted to narrow bands within intra-annual band. There
544 is a significant variation in the strength of intra-annual variability ([Fig. 13](#)) and its component
545 ([Fig. 7](#)) with time. For example, off Goa at 40 m during September to November of 2020 and
546 2022, the intra-annual component is weak and strong, respectively ([Fig. 13](#)). This difference is due

547 to the spread of energy among all intra-annual periods for 2022 ([Fig. 7](#)), while during 2020 the
548 wavelet energy is only present in the semi-annual periods, resulting in a overall weaker intra-annual
549 component. For the same reason, the intra-annual variability is non-existent in 2019.

550 The intraseasonal band, defined as the variability occurring between periods of few days to 90
551 days is split into two categories; a high-frequency (period < 30 days) and a low-frequency (30 <
552 period < 90 days) component. The presence of low-frequency intraseasonal signals is observed in
553 the wavelet analysis of biomass at 40 m ([Fig. 7](#)) and 104 m ([Fig. 8](#)) as bursts during few months
554 distinctive to each mooring location. The wavelet power at 40 m in low-frequency intraseasonal
555 band peaks during September to December off Mumbai, Jaigarh and Kanyakumari while no such
556 general observation is found in other locations. However, the wavelet power at 104 m in comparison
557 to 40 m suggests a decrease in its strength at respective locations. Lanczos filtered biomass in 30 to
558 90 day period shows that the intraseasonal variability is strong during August to November off all
559 location ([Fig. 14](#)). This is in contrast to the WICC intraseasonal band which is strong during winter
560 monsoon [[Amol et al., 2014](#), [Chaudhuri et al., 2020](#)]. The low frequency intraseasonal variability
561 is higher in the upper ocean, however it can extend to deeper depths (~ 140) for some years
562 e.g, off Kollam during 2022 ([Fig. 14 f](#)). The magnitude of low-frequency intraseasonal component
563 is high as we move equatorward till Kollam and declines off Kanyakumari ([Fig. 14 g](#)). As noted
564 earlier in variability of the intra-annual component, the intra-seasonal component's strength and its
565 variability is transient in nature, and the intra-seasonal variation has implication on the zooplankton
566 sampling.

567 **4.4 Discussion**

568 Numerous oceanic factors have an impact on the zooplankton population dynamics and growth
569 in the Eastern Arabian Sea. Throughout the summer monsoon, the Somali Current, which flows
570 clockwise, is essential in moving oxygen-depleted waters the Arabian Sea creating a perennial oxygen
571 minimum zone (OMZ) that lasts forever in the area. [Kim et al., 2018, Sarma et al., 2020, Sudheesh
572 et al., 2022]. Upwelling supplies nutrients to the surface [Kumar et al., 2000], but it also plays a
573 role in the creation of hypoxic conditions, which can restrict the kinds of zooplankton species that
574 can survive in these waters [Jayakumar et al., 2004]. The upwelling starts in early, by February
575 itself off SEAS, but it occurs much later during May farther north along the coast [Banse, 1968,
576 Kumar et al., 2000, Sarma et al., 2020]. The deepening of MLD in winter [Marra and Barber,
577 2005, Shankar et al., 2016, Shi and Wang, 2022] leads to dilution of zooplankton grazers [Marra
578 and Barber, 2005] and hence longer food chain [Banse, 1995, Barber et al., 2001], explaining the
579 carnivorous dominated fisheries in NEAS [Shankar et al., 2019] and herbivore dominated SEAS
580 [Longhurst and Wooster, 1990, Shankar et al., 2019].

581 **References**

- 582 Anna-Karin Almén and Tobias Tamelander. Temperature-related timing of the spring bloom and match between
583 phytoplankton and zooplankton. *Marine Biology Research*, 16(8-9):674–682, 2020.
- 584 P Amol, D Shankar, V Fernando, A Mukherjee, SG Aparna, R Fernandes, GS Michael, ST Khalap, NP Satelkar,
585 Y Agarvadekar, et al. Observed intraseasonal and seasonal variability of the west india coastal current on the
586 continental slope. *Journal of Earth System Science*, 123(5):1045–1074, 2014.
- 587 P Amol, Suchandan Bemal, D Shankar, V Jain, V Thushara, V Vijith, and PN Vinayachandran. Modulation of
588 chlorophyll concentration by downwelling rossby waves during the winter monsoon in the southeastern arabian
589 sea. *Progress in Oceanography*, 186:102365, 2020.
- 590 SG Aparna, DV Desai, D Shankar, AC Anil, Shrikant Dora, and R Khedekar. Seasonal cycle of zooplankton standing
591 stock inferred from adcp backscatter measurements in the eastern arabian sea. *Progress in Oceanography*, 203:
592 102766, 2022.

- 593 Carin J Ashjian, Sharon L Smith, Charles N Flagg, and Nasseer Idrisi. Distribution, annual cycle, and vertical
594 migration of acoustically derived biomass in the arabian sea during 1994–1995. *Deep Sea Research Part II: Topical Studies in Oceanography*, 49(12):2377–2402, 2002.
- 596 K Banse and DC English. Geographical differences in seasonality of czcs-derived phytoplankton pigment in the
597 arabian sea for 1978–1986. *Deep Sea Research Part II: Topical Studies in Oceanography*, 47(7-8):1623–1677, 2000.
- 598 Karl Banse. Hydrography of the arabian sea shelf of india and pakistan and effects on demersal fishes. In *Deep sea*
599 *research and oceanographic Abstracts*, volume 15, pages 45–79. Elsevier, 1968.
- 600 Karl Banse. Zooplankton: pivotal role in the control of ocean production: I. biomass and production. *ICES Journal*
601 *of marine Science*, 52(3-4):265–277, 1995.
- 602 Richard T Barber, John Marra, Robert C Bidigare, Louis A Codispoti, David Halpern, Zackary Johnson, Mikel
603 Latasa, Ralf Goericke, and Sharon L Smith. Primary productivity and its regulation in the arabian sea during
604 1995. *Deep Sea Res. Part 2 Top. Stud. Oceanogr.*, 48(6-7):1127–1172, jan 2001.
- 605 WE Barraclough, RJ LeBrasseur, and OD Kennedy. Shallow scattering layer in the subarctic pacific ocean: detection
606 by high-frequency echo sounder. *Science*, 166(3905):611–613, 1969.
- 607 H. P. Batchelder, J. R. VanKeuren, R. D. Vaillancourt, and E. Swift. Spatial and temporal distributions of acoustically
608 estimated zooplankton biomass near the marine light-mixed layers station ($59^{\circ}30'N$, $21^{\circ}00'W$) in the north atlantic
609 in may 1991. *Journal of Geophysical Research: Oceans*, 100:6549–6563, 1995. doi: 10.1029/94jc00981.
- 610 John C Brock and Charles R McClain. Interannual variability in phytoplankton blooms observed in the northwestern
611 arabian sea during the southwest monsoon. *Journal of Geophysical Research: Oceans*, 97(C1):733–750, 1992.
- 612 John C Brock, Charles R McClain, Mark E Luther, and William W Hay. The phytoplankton bloom in the north-
613 western arabian sea during the southwest monsoon of 1979. *Journal of Geophysical Research: Oceans*, 96(C11):
614 20623–20642, 1991.
- 615 Abhisek Chatterjee, D Shankar, SSC Shenoi, GV Reddy, GS Michael, M Ravichandran, VV Gopalkrishna,
616 EP Rama Rao, TVS Udaya Bhaskar, and VN Sanjeevan. A new atlas of temperature and salinity for the north
617 indian ocean. *Journal of Earth System Science*, 121:559–593, 2012.
- 618 Anya Chaudhuri, D Shankar, SG Aparna, P Amol, V Fernando, A Kankonkar, GS Michael, NP Satelkar, ST Khalap,
619 AP Tari, et al. Observed variability of the west india coastal current on the continental slope from 2009–2018.
620 *Journal of Earth System Science*, 129(1):57, 2020.
- 621 Anya Chaudhuri, P Amol, D Shankar, S Mukhopadhyay, SG Aparna, V Fernando, and A Kankonkar. Observed
622 variability of the west india coastal current on the continental shelf from 2010–2017. *Journal of Earth System*
623 *Science*, 130:1–21, 2021.

- 624 Boris Cisewski, Volker H Strass, Monika Rhein, and Sören Krägesky. Seasonal variation of diel vertical migration
625 of zooplankton from adcp backscatter time series data in the lazarev sea, antarctica. *Deep Sea Research Part I: Oceanographic Research Papers*, 57(1):78–94, 2010.
- 627 Kent L Deines. Backscatter estimation using broadband acoustic doppler current profilers. In *Proceedings of the IEEE Sixth Working Conference on Current Measurement (Cat. No. 99CH36331)*, pages 249–253. IEEE, 1999.
- 629 A Edvardsen, D Slagstad, KS Tande, and P Jaccard. Assessing zooplankton advection in the barents sea using
630 underway measurements and modelling. *Fisheries Oceanography*, 12(2):61–74, 2003.
- 631 S Fielding, G Griffiths, and HSJ Roe. The biological validation of adcp acoustic backscatter through direct comparison
632 with net samples and model predictions based on acoustic-scattering models. *ICES Journal of Marine Science*,
633 61(2):184–200, 2004.
- 634 Charles N Flagg and Sharon L Smith. On the use of the acoustic doppler current profiler to measure zooplankton
635 abundance. *Deep Sea Research Part A. Oceanographic Research Papers*, 36(3):455–474, 1989.
- 636 Kevin D Friedland, Charles Stock, Kenneth F Drinkwater, Jason S Link, Robert T Leaf, Burton V Shank, Julie M
637 Rose, Cynthia H Pilskaln, and Michael J Fogarty. Pathways between primary production and fisheries yields of
638 large marine ecosystems. *PloS one*, 7(1):e28945, 2012.
- 639 H. E. García, R. A. Locarnini, T. P. Boyer, J. I. Antonov, A. V. Mishonov, O. K. Baranova, M. M. Zweng, J. R.
640 Reagan, and D. R. Johnson. Dissolved oxygen, apparent oxygen utilization, and oxygen saturation. *NOAA Atlas NESDIS 75*, 3, 2014.
- 642 Charles H Greene, Peter H Wiebe, Chris Pelkie, Mark C Benfield, and Jacqueline M Popp. Three-dimensional
643 acoustic visualization of zooplankton patchiness. *Deep Sea Research Part II: Topical Studies in Oceanography*, 45
644 (7):1201–1217, 1998.
- 645 Charles F Greenlaw. Acoustical estimation of zooplankton populations 1. *Limnology and Oceanography*, 24(2):
646 226–242, 1979.
- 647 Davide Guerra, Katrin Schroeder, Mireno Borghini, Elisa Camatti, Marco Pansera, Anna Schroeder, Stefania
648 Sparnocchia, and Jacopo Chiggiato. Zooplankton diel vertical migration in the corsica channel (north-western
649 mediterranean sea) detected by a moored acoustic doppler current profiler. *Ocean Science*, 15(3):631–649, 2019.
- 650 James M Hamilton, Kate Collins, and Simon J Prinsenberg. Links between ocean properties, ice cover, and plankton
651 dynamics on interannual time scales in the canadian arctic archipelago. *Journal of Geophysical Research: Oceans*,
652 118(10):5625–5639, 2013.
- 653 Graeme C Hays. A review of the adaptive significance and ecosystem consequences of zooplankton diel vertical
654 migrations. In *Migrations and Dispersal of Marine Organisms: Proceedings of the 37 th European Marine Biology
655 Symposium held in Reykjavík, Iceland, 5–9 August 2002*, pages 163–170. Springer, 2003.

- 656 PJ Herring, MJR Fasham, AR Weeks, JCP Hemmings, HSJ Roe, PR Pugh, S Holley, NA Crisp, and MV Angel.
657 Across-slope relations between the biological populations, the euphotic zone and the oxygen minimum layer off
658 the coast of oman during the southwest monsoon (august, 1994). *Progress in Oceanography*, 41(1):69–109, 1998.
- 659 Karen J Heywood, S Scrope-Howe, and ED Barton. Estimation of zooplankton abundance from shipborne adcp
660 backscatter. *Deep Sea Research Part A. Oceanographic Research Papers*, 38(6):677–691, 1991.
- 661 Laura Hobbs, Neil S Banas, Jonathan H Cohen, Finlo R Cottier, Jørgen Berge, and Øystein Varpe. A marine
662 zooplankton community vertically structured by light across diel to interannual timescales. *Biology Letters*, 17(2):
663 20200810, 2021.
- 664 Raleigh R Hood, Lynnath E Beckley, and Jerry D Wiggert. Biogeochemical and ecological impacts of boundary
665 currents in the indian ocean. *Progress in Oceanography*, 156:290–325, 2017.
- 666 Ryuichiro Inoue, Minoru Kitamura, and Tetsuichi Fujiki. Diel vertical migration of zooplankton at the s 1 biogeo-
667 chemical mooring revealed from acoustic backscattering strength. *Journal of Geophysical Research: Oceans*, 121
668 (2):1031–1050, 2016.
- 669 D. A. Jayakumar, Christopher A. Francis, S.W.A. Naqvi, and Bess B. Ward. Diversity of nitrite reductase genes
670 (nirs) in the denitrifying water column of the coastal arabian sea. *Aquatic Microbial Ecology*, 2004. doi: 10.3354/
671 ame034069.
- 672 Songnian Jiang, Tommy D Dickey, Deborah K Steinberg, and Laurence P Madin. Temporal variability of zooplankton
673 biomass from adcp backscatter time series data at the bermuda testbed mooring site. *Deep Sea Research Part I:*
674 *Oceanographic Research Papers*, 54(4):608–636, 2007.
- 675 R Jyothibabu, NV Madhu, H Habeebrehman, KV Jayalakshmy, KKC Nair, and CT Achuthankutty. Re-evaluation
676 of ‘paradox of mesozooplankton’ in the eastern arabian sea based on ship and satellite observations. *Journal of*
677 *Marine Systems*, 81(3):235–251, 2010.
- 678 Myounghee Kang, Sunyoung Oh, Wooseok Oh, Dong-Jin Kang, SungHyun Nam, and Kyounghoon Lee. Acoustic
679 characterization of fish and macroplankton communities in the seychelles-chagos thermocline ridge of the southwest
680 indian ocean. *Deep Sea Research Part II: Topical Studies in Oceanography*, 213:105356, 2024.
- 681 Madhavan Girijakumari Keerthi, Matthieu Lengaigne, Marina Levy, Jerome Vialard, Vallivattathillam Parvathi,
682 Clément de Boyer Montégut, Christian Ethé, Olivier Aumont, Iyyappan Suresh, Valiya Parambil Akhil, et al.
683 Physical control of interannual variations of the winter chlorophyll bloom in the northern arabian sea. *Bioge-
684osciences*, 14(15):3615–3632, 2017.
- 685 Punam A Khandagale, Vaibhav D Mhatre, and Sujitha Thomas. Seasonal and spatial variability of zooplankton
686 diversity in north eastern arabian sea along the maharashtra coast. *Journal of the Marine Biological Association*
687 *of India*, 64(1):25–32, 2022.
- 688 S Kidwai and S Amjad. Zooplankton: pre-southwest and northeast monsoons of 1993 to 1994, from the north arabian
689 sea. *Mar. Biol.*, 136(3):561–571, apr 2000.

- 690 Jieun Kim, Boo-Keun Khim, Minoru Ikebara, and Jongmin Lee. Orbital-scale denitrification changes in the eastern
691 arabian sea during the last 800 kyrs. *Scientific Reports*, 2018. doi: 10.1038/s41598-018-25415-7.
- 692 S. Prasanna Kumar, M. Madhupratap, M. Dileep Kumar, Mangesh Gauns, P.M. Muraleedharan, V. V. S. S. Sarma,
693 and Sílvia Naves de Souza. Physical control of primary productivity on a seasonal scale in central and eastern
694 arabian sea. *Journal of Earth System Science*, 2000. doi: 10.1007/bf02708331.
- 695 Corinne Le Qu, Robbie M Andrew, Josep G Canadell, Stephen Sitch, Jan Ivar Korsbakken, Glen P Peters, Andrew C
696 Manning, Thomas A Boden, Pieter P Tans, Richard A Houghton, et al. Global carbon budget 2016. *Earth System
697 Science Data*, 8(2):605–649, 2016.
- 698 Marina Lévy, D Shankar, J-M André, SSC Shenoi, Fabien Durand, and Clément de Boyer Montégut. Basin-wide
699 seasonal evolution of the indian ocean's phytoplankton blooms. *Journal of Geophysical Research: Oceans*, 112
700 (C12), 2007.
- 701 M Li, A Gargett, and K Denman. What determines seasonal and interannual variability of phytoplankton and
702 zooplankton in strongly estuarine systems? *Estuarine, Coastal and Shelf Science*, 50(4):467–488, 2000.
- 703 Yanliang Liu, Jingsong Guo, Yuhuan Xue, Chalermrat Sangmanee, Huiwu Wang, Chang Zhao, Somkiat Khokiat-
704 tiwong, and Weidong Yu. Seasonal variation in diel vertical migration of zooplankton and micronekton in the
705 andaman sea observed by a moored adcp. *Deep Sea Research Part I: Oceanographic Research Papers*, 179:103663,
706 2022.
- 707 Alan R Longhurst and Warren S Wooster. Abundance of oil sardine (*sardinella longiceps*) and upwelling on the
708 southwest coast of india. *Can. J. Fish. Aquat. Sci.*, 47(12):2407–2419, dec 1990.
- 709 M Madhupratap, P Haridas, Neelam Ramaiah, and CT Achuthankutty. Zooplankton of the southwest coast of india:
710 abundance, composition, temporal and spatial variability in 1987. 1992.
- 711 M Madhupratap, TC Gopalakrishnan, P Haridas, KKC Nair, PN Aravindakshan, G Padmavati, and Shiney Paul.
712 Lack of seasonal and geographic variation in mesozooplankton biomass in the arabian sea and its structure in the
713 mixed layer. *Current science. Bangalore*, 71(11):863–868, 1996a.
- 714 M Madhupratap, S Prasanna Kumar, PMA Bhattathiri, M Dileep Kumar, S Raghukumar, KKC Nair, and N Rama-
715 iah. Mechanism of the biological response to winter cooling in the northeastern arabian sea. *Nature*, 384(6609):
716 549–552, 1996b.
- 717 M Madhupratap, TC Gopalakrishnan, P Haridas, and KKC Nair. Mesozooplankton biomass, composition and
718 distribution in the arabian sea during the fall intermonsoon: implications of oxygen gradients. *Deep Sea Research
719 Part II: Topical Studies in Oceanography*, 48(6-7):1345–1368, 2001.
- 720 PA Maheswaran, G Rajesh, C Revichandran, and KKC Nair. Upwelling and associated hydrography along the west
721 coast of india during southwest monsoon, 1999. 2000.

- 722 Douglas Maraun and Jürgen Kurths. Cross wavelet analysis: significance testing and pitfalls. *Nonlinear Processes*
723 in *Geophysics*, 11(4):505–514, 2004.
- 724 John Marra and Richard T. Barber. Primary productivity in the arabian sea: A synthesis of jgofs data. *Progress*
725 in *Oceanography*, 65(2):159–175, 2005. ISSN 0079-6611. doi: <https://doi.org/10.1016/j.pocean.2005.03.004>. URL
726 <https://www.sciencedirect.com/science/article/pii/S007966110500042X>. The Arabian Sea of the 1990s: New
727 Biogeochemical Understanding.
- 728 JP McCreary, Raghu Murtugudde, Jerome Vialard, PN Vinayachandran, Jerry D Wiggert, Raleigh R Hood,
729 D Shankar, and S Shetye. Biophysical processes in the indian ocean. *Indian Ocean biogeochemical processes*
730 and *ecological variability*, 185:9–32, 2009.
- 731 Julian P McCreary Jr, Pijush K Kundu, and Robert L Molinari. A numerical investigation of dynamics, thermody-
732 namics and mixed-layer processes in the indian ocean. *Progress in Oceanography*, 31(3):181–244, 1993.
- 733 Donald C McNaught. Acoustical determination of zooplankton distribution. In *Proc. 11th Conf. Great lakes Res.*,
734 pages 76–84, 1968.
- 735 A Mukherjee, D Shankar, V Fernando, P Amol, SG Aparna, R Fernandes, GS Michael, ST Khalap, NP Satelkar,
736 Y Agarvadekar, et al. Observed seasonal and intraseasonal variability of the east india coastal current on the
737 continental slope. *Journal of Earth System Science*, 123(6):1197–1232, 2014.
- 738 S Mukhopadhyay, D Shankar, SG Aparna, A Mukherjee, V Fernando, A Kankonkar, S Khalap, NP Satelkar,
739 MG Gaonkar, AP Tari, et al. Observed variability of the east india coastal current on the continental slope
740 during 2009–2018. *Journal of Earth System Science*, 129:1–22, 2020.
- 741 Jerry Mullison. Backscatter estimation using broadband acoustic doppler current profilers-updated. In *Proceedings*
742 of the ASCE Hydraulic Measurements & Experimental Methods Conference, Durham, NH, USA, pages 9–12,
743 2017.
- 744 KKC Nair, M Madhupratap, TC Gopalakrishnan, P Haridas, and Mangesh Gauns. The arabian sea: physical
745 environment, zooplankton and myctophid abundance. 1999.
- 746 PV Nair. Primary productivity in the indian seas. *CMFRI Bulletin*, 22:1–63, 1970.
- 747 D Nethery and D Shankar. Vertical propagation of baroclinic kelvin waves along the west coast of india. *J. Earth*
748 *Syst. Sci.*, 116(4):331–339, aug 2007.
- 749 Lingyun Nie, Jianchao Li, Hao Wu, Wencho Zhang, Yongjun Tian, Yang Liu, Peng Sun, Zhenjiang Ye, Shuyang
750 Ma, and Qinfeng Gao. The influence of ocean processes on fine-scale changes in the yellow sea cold water mass
751 boundary area structure based on acoustic observations. *Remote Sensing*, 15(17):4272, 2023.
- 752 MD Ohman and H-J Hirche. Density-dependent mortality in an oceanic copepod population. *Nature*, 412(6847):
753 638–641, 2001.

- 754 G Padmavati, P Haridas, KKC Nair, TC Gopalakrishnan, P Shiney, and M Madhupratap. Vertical distribution of
755 mesozooplankton in the central and eastern arabian sea during the winter monsoon. *Journal of Plankton Research*,
756 20(2):343–354, 1998.
- 757 MR Patil, CP Ramamirtham, P Udaya Varma, and CP Nair. Hydrography of the west coast of india during the
758 pre-monsoon period of the year 1962. *Journal of marine biological association of India*, 6(1):151–164, 1964.
- 759 Richard Edward Pieper. *A study of the relationship between zooplankton and high-frequency scattering of underwater*
760 *sound*. PhD thesis, University of British Columbia, 1971.
- 761 SA Piontkovski, R Williams, and TA Melnik. Spatial heterogeneity, biomass and size structure of plankton of the
762 indian ocean: some general trends. *Marine ecology progress series*, pages 219–227, 1995.
- 763 Emmanuel Potiris, Constantin Frangoulis, Alkiviadis Kalampokis, Manolis Ntoumas, Manos Pettas, George Peti-
764 hakis, and Vassilis Zervakis. Acoustic doppler current profiler observations of migration patterns of zooplankton
765 in the cretan sea. *Ocean Science*, 14(4):783–800, 2018.
- 766 SZ Qasim. Biological productivity of the indian ocean. 1977.
- 767 CP Ramamirtham and AVS Murty. Hydrography of the west coast of india during the pre-monsoon period of the
768 year 1962—part 2: in and offshore waters of the konkan and malabar coasts. *Journal of the Marine Biological*
769 *Association of India*, 7(1):150–168, 1965.
- 770 S Ramamurthy. Studies on the plankton of the north kanara coast in relation to the pelagic fishery. *Journal of*
771 *Marine Biological Association of India*, 7(1):127–149, 1965.
- 772 Mehbuba Rehim and Mudassar Imran. Dynamical analysis of a delay model of phytoplankton–zooplankton interac-
773 *tion*. *Applied Mathematical Modelling*, 36(2):638–647, 2012.
- 774 T. P. Rippeth and J. H. Simpson. Diurnal signals in vertical motions on the hebridean shelf. *Limnology and*
775 *Oceanography*, 43:1690–1696, 1998. doi: 10.4319/lo.1998.43.7.1690.
- 776 John H Ryther, John R Hall, Allan K Pease, Andrew Bakun, and Mark M Jones. Primary organic production in
777 relation to the chemistry and hydrography of the western indian ocean 1. *Limnology and Oceanography*, 11(3):
778 371–380, 1966.
- 779 D Sameoto and S Paulowich. The use of 120 khz sonar in zooplankton studies. In *OCEANS'77 Conference Record*,
780 pages 523–528. IEEE, 1977.
- 781 VVSS Sarma, TVS Udaya Bhaskar, J Pavan Kumar, and Kunal Chakraborty. Potential mechanisms responsible for
782 occurrence of core oxygen minimum zone in the north-eastern arabian sea. *Deep Sea Research Part I: Oceano-*
783 *graphic Research Papers*, 165:103393, 2020.
- 784 D Shankar and SR Shetye. On the dynamics of the lakshadweep high and low in the southeastern arabian sea.
785 *Journal of Geophysical Research: Oceans*, 102(C6):12551–12562, 1997.

- 786 D Shankar, R Remya, PN Vinayachandran, Abhisek Chatterjee, and Ambica Behera. Inhibition of mixed-layer
787 deepening during winter in the northeastern arabian sea by the west india coastal current. *Climate Dynamics*,
788 47:1049–1072, 2016.
- 789 D Shankar, R Remya, AC Anil, and V Vijith. Role of physical processes in determining the nature of fisheries in the
790 eastern arabian sea. *Progress in Oceanography*, 172:124–158, 2019.
- 791 SR Shetye and AD Gouveia. Coastal circulation in the north indian ocean: Coastal segment (14, sw). John Wiley
792 and Sons, New York, USA, 1998.
- 793 SR Shetye, AD Gouveia, SSC Shenoi, D Sundar, GS Michael, AM Almeida, and K Santanam. Hydrography and
794 circulation off the west coast of india during the southwest monsoon 1987. 1990.
- 795 SR Shetye, AD Gouveia, SSC Shenoi, GS Michael, D Sundar, AM Almeida, and K Santanam. The coastal current
796 off western india during the northeast monsoon. *Deep Sea Research Part A. Oceanographic Research Papers*, 38
797 (12):1517–1529, 1991.
- 798 SR Shetye, AD Gouveia, and SSC Shenoi. Does winter cooling lead to the subsurface salinity minimum off saurashtra,
799 india? *Oceanography of the Indian Ocean*, pages 617–625, 1992.
- 800 Wei Shi and Menghua Wang. Phytoplankton biomass dynamics in the arabian sea from viirs observations. *Journal
801 of Marine Systems*, 227:103670, 2022.
- 802 Greg M Silsbe, Michael J Behrenfeld, Kimberly H Halsey, Allen J Milligan, and Toby K Westberry. The cafe model:
803 A net production model for global ocean phytoplankton. *Global Biogeochemical Cycles*, 30(12):1756–1777, 2016.
- 804 Houssem Smeti, Marc Pagano, Christophe Menkes, Anne Lebourges-Dhaussy, Brian PV Hunt, Valerie Allain, Martine
805 Rodier, Florian De Boissieu, Elodie Kestenare, and Cherif Sammari. Spatial and temporal variability of zooplankton
806 off n ew c aledonia (s outhwestern p acific) from acoustics and net measurements. *Journal of Geophysical
807 Research: Oceans*, 120(4):2676–2700, 2015.
- 808 SL Smith and M Madhupratap. Mesozooplankton of the arabian sea: patterns influenced by seasons, upwelling, and
809 oxygen concentrations. *Progress in Oceanography*, 65(2-4):214–239, 2005.
- 810 Patnaik Sreenivas, KVKRK Patnaik, and KVSR Prasad. Monthly variability of mixed layer over arabian sea using
811 argo data. *Marine Geodesy*, 31(1):17–38, 2008.
- 812 R Subrahmanyam. Studies on the phytoplankton of the west coast of india: Part ii. physical and chemical factors
813 influencing the production of phytoplankton, with remarks on the cycle of nutrients and on the relationship of
814 the phosphate-content to fish landings. In *Proceedings/Indian Academy of Sciences*, volume 50, pages 189–252.
815 Springer, 1959.
- 816 R Subrahmanyam and AH Sarma. Studies on the phytoplankton of the west coast of india. part iii. seasonal variation
817 of the phytoplankters and environmental factors. *Indian Journal of Fisheries*, 7(2):307–336, 1960.

- 818 V. Sudheesh, G.V.M. Gupta, Yudhishtir Reddy, Kausar F. Bepari, N.V.H.K. Chari, C.K. Sherin, S.S. Shaju, Ch.V.
819 Ramu, and Anil Kumar Vijayan. Oxygen minimum zone along the eastern arabian sea: Intra-annual varia-
820 tion and dynamics based on ship-borne studies. *Progress in Oceanography*, 201:102742, 2022. ISSN 0079-6611.
821 doi: <https://doi.org/10.1016/j.pocean.2022.102742>. URL <https://www.sciencedirect.com/science/article/pii/S0079661122000040>.
- 823 Laura Ursella, Vanessa Cardin, Mirna Batistić, Rade Garić, and Miroslav Gačić. Evidence of zooplankton vertical
824 migration from continuous southern adriatic buoy current-meter records. *Progress in oceanography*, 167:78–96,
825 2018.
- 826 Laura Ursella, Sara Pensieri, Enric Pallàs-Sanz, Sharon Z Herzka, Roberto Bozzano, Miguel Tenreiro, Vanessa Cardin,
827 Julio Candela, and Julio Sheinbaum. Diel, lunar and seasonal vertical migration in the deep western gulf of mexico
828 evidenced from a long-term data series of acoustic backscatter. *Progress in Oceanography*, 195:102562, 2021.
- 829 V Vijith, PN Vinayachandran, V Thushara, P Amol, D Shankar, and AC Anil. Consequences of inhibition of mixed-
830 layer deepening by the west india coastal current for winter phytoplankton bloom in the northeastern arabian sea.
831 *Journal of Geophysical Research: Oceans*, 121(9):6583–6603, 2016.
- 832 Peter H Wiebe, Charles H Greene, Timothy K Stanton, and Janusz Burczynski. Sound scattering by live zooplankton
833 and micronekton: empirical studies with a dual-beam acoustical system. *The Journal of the Acoustical Society of
834 America*, 88(5):2346–2360, 1990.
- 835 Monika Winder and Daniel E Schindler. Climatic effects on the phenology of lake processes. *Global change biology*,
836 10(11):1844–1856, 2004.
- 837 Karen F Wishner, Marcia M Gowing, and Celia Gelfman. Mesozooplankton biomass in the upper 1000 m in the
838 arabian sea: overall seasonal and geographic patterns, and relationship to oxygen gradients. *Deep Sea Research
839 Part II: Topical Studies in Oceanography*, 45(10-11):2405–2432, 1998.

Table 1: ADCP deployment details at the locations. The temporal resolution is 1 hour, bin size(vertical resolution) 4 m. All ADCPs are operated at 153.3 kHz. The moorings are at a water column depth of 950 - 1200 m on the continental slope and are serviced on yearly basis according to ship availability. The 6th column consists of Reference echo intensity (Er) for each beam, while the 7th column contains the corresponding RSSI conversion factor [Deines, 1999].

Station (Position; $^{\circ}$ E, $^{\circ}$ N)	Date		Depth			
	Deployment	Recovery	Ocean	ADCP	Er	Kc
Okha (67.47, 22.26)	01/10/2018	01/12/2019	996	118	37 , 37 , 37 , 36	0.42 , 0.44 , 0.42 , 0.43
	01/12/2019	04/12/2020	1166	312	39 , 36 , 38 , 36	0.42 , 0.44 , 0.42 , 0.43
	04/12/2020	08/03/2022	1021	144	41 , 37 , 38 , 37	0.42 , 0.44 , 0.42 , 0.43
	08/03/2022	01/01/2023	1019	142	37 , 38 , 39 , 36	0.42 , 0.44 , 0.42 , 0.43
Mumbai (69.24, 20.01)	09/11/2017	29/09/2018	1025	150	36 , 34 , 39 , 42	0.40 , 0.40 , 0.40 , 0.40
	29/09/2018	29/11/2019	1122	125	35 , 36 , 39 , 42	0.40 , 0.40 , 0.40 , 0.40
	29/11/2019	02/12/2020	1143	164	37 , 34 , 39 , 43	0.40 , 0.40 , 0.40 , 0.40
	02/12/2020	06/03/2022	1125	142	36 , 34 , 39 , 42	0.40 , 0.40 , 0.40 , 0.40
	07/03/2022	02/01/2023	1103	158	37 , 34 , 40 , 43	0.40 , 0.40 , 0.40 , 0.40
Jaigarh (71.12, 17.53)	27/10/2017	27/09/2018	1039	198	32 , 35 , 33 , 32	0.45 , 0.45 , 0.45 , 0.45
	27/09/2018	30/10/2019	1032	164	32 , 35 , 33 , 31	0.45 , 0.45 , 0.45 , 0.45
	03/11/2019	30/11/2020	1142	264	32 , 36 , 33 , 32	0.45 , 0.45 , 0.45 , 0.45
	30/11/2020	05/03/2022	1099	119	33 , 36 , 34 , 32	0.45 , 0.45 , 0.45 , 0.45
Goa (72.74, 15.17)	03/10/2017	25/09/2018	1000	174	35 , 37 , 34 , 35	0.44 , 0.44 , 0.40 , 0.41
	25/09/2018	16/10/2019	969	145	38 , 36 , 36 , 34	0.44 , 0.44 , 0.40 , 0.41
	16/10/2019	29/11/2020	966	143	44 , 38 , 36 , 43	0.44 , 0.44 , 0.40 , 0.41
	29/11/2020	03/03/2022	985	157	35 , 40 , 35 , 38	0.44 , 0.44 , 0.40 , 0.41
	03/03/2022	05/01/2023	984	159	35 , 38 , 35 , 34	0.44 , 0.44 , 0.40 , 0.41
Udupi (74.04, 12.5)	05/10/2017	06/10/2018	1028	176	44 , 46 , 29 , 35	0.45 , 0.45 , 0.45 , 0.45
	06/10/2018	18/10/2019	1027	179	32 , 38 , 30 , 36	0.45 , 0.45 , 0.45 , 0.45
	18/10/2019	11/12/2020	1018	168	33 , 37 , 31 , 38	0.45 , 0.45 , 0.45 , 0.45
	11/03/2022	06/01/2023	1036	155	31 , 32 , 32 , 33	0.45 , 0.45 , 0.45 , 0.45
Kollam (75.44, 9.05)	07/10/2017	08/10/2018	1174	200	43 , 55 , 45 , 43	0.49 , 0.50 , 0.49 , 0.50
	08/10/2018	20/10/2019	1160	123	49 , 62 , 46 , 46	0.49 , 0.50 , 0.49 , 0.50
	20/10/2019	13/12/2020	1209	176	52 , 61 , 54 , 55	0.49 , 0.50 , 0.49 , 0.50
	13/12/2020	13/03/2022	1129	91	49 , 51 , 46 , 47	0.49 , 0.50 , 0.49 , 0.50
	13/03/2022	08/01/2023	1149	164	41 , 48 , 43 , 41	0.49 , 0.50 , 0.49 , 0.50
Kanyakumari (77.39, 6.96)	16/11/2016	08/10/2017	1096	252	37 , 36 , 37 , 37	0.42 , 0.44 , 0.42 , 0.43
	08/10/2017	10/10/2018	1055	181	32 , 34 , 38 , 35	0.45 , 0.45 , 0.45 , 0.45
	10/10/2018	22/10/2019	1075	180	36 , 34 , 39 , 36	0.45 , 0.45 , 0.45 , 0.45
	22/10/2019	14/12/2020	1060	167	33 , 35 , 36 , 35	0.45 , 0.45 , 0.45 , 0.45
	14/12/2020	14/03/2022	1184	287	34 , 36 , 36 , 35	0.45 , 0.45 , 0.45 , 0.45

Table 2:

Volumetric samples of zooplankton of various stations. The sampling depth range is standardised for later years for bin range of 0–25m, 25–50m, 50–75m, 75–100m, 100–150m. The abbreviations are in the following manner: Okha (O), Mumbai (M), Jaigarh (J), Goa (G), Udupi (U), Kollam (K), Kanyakumari (KK); The number tags corresponds to particular cruise of a station.

Sample number	Tag	Lat($^{\circ}$ N)	Lon($^{\circ}$ E)	Date	Time (IST)	Sampling depth range (m)
1-3	G1	15.18	72.79	25 Sep 18	452	50–25, 100–50, 150–100
4-6	G2	15.16	72.71	25 Sep 18	2108	50–25, 100–50, 150–100
7-10	G2	15.16	72.71	25 Sep 18	2137	40–20, 60–40, 80–60, 100–80
11-14	J1			26 Sep 18	2000	40–20, 60–40, 80–60, 100–80
15-17	J2			27 Sep 18	2000	50–25, 100–50, 150–100
18-21	J2			27 Sep 18	2100	40–20, 60–40, 80–60, 100–80
22-25	M1	20	69.19	28 Sep 18	2135	40–20, 60–40, 80–60, 100–80
26-27	M1	20	69.19	28 Sep 18	2205	50–25, 100–50
28-29	M2	20.01	69.2	29 Sep 18	2035	50–25, 100–50
30-33	M2	20.01	69.2	29 Sep 18	2057	40–20, 60–40, 80–60, 100–80
34-37	U1			5 Oct 18	2000	40–20, 60–40, 80–60, 100–80
38-40	U1			5 Oct 18	2100	50–25, 100–50, 150–100
41-43	U2			6 Oct 18	2000	50–25, 100–50, 150–100
44-47	U2			6 Oct 18	2100	40–20, 60–40, 80–60, 100–80
48-51	K1	9.06	75.42	8 Oct 18	421	40–20, 60–40, 80–60, 100–80
52-54	K1	9.06	75.42	8 Oct 18	449	50–25, 100–50, 150–100
55-56	K2	9.04	75.4	8 Oct 18	2027	50–25, 100–50
57-60	K2	9.04	75.4	8 Oct 18	2045	40–20, 60–40, 80–60, 100–80
61-64	G2	15.16	72.74	16 Oct 19	829	50–25, 75–50, 100–75, 150–100
65-67	G3	15.16	72.74	16 Oct 19	1812	50–25, 75–50, 100–75
68-70	K2	9.02	75.42	20 Oct 19	840	50–25, 75–50, 100–75
71-74	K3	9.04	75.43	20 Oct 19	1934	50–25, 75–50, 100–75, 150–100
75-78	KK1			22 Oct 19	742	50–25, 75–50, 100–75, 150–100
79-82	KK2			22 Oct 19	1925	50–25, 75–50, 100–75, 150–100
83-86	J1			30 Oct 19	324	50–25, 75–50, 100–75, 150–100
87-89	J2			4 Nov 19	946	75–50, 100–75, 150–100
90-92	M2	19.98	69.22	29 Nov 19	1434	50–25, 75–50, 100–75
93-96	M3	20.01	69.23	30 Nov 19	958	50–25, 75–50, 100–75, 150–100
97-100	O1	22.24	67.49	1 Dec 19	937	50–25, 75–50, 100–75, 150–100
101	O2	22.25	67.46	1 Dec 19	1957	150–100
102-105	G3	15.68	73.22	28 Nov 20	930	50–25, 75–50, 100–75, 150–100
105-108	G4	15.32	73.22	29 Nov 20	1558	50–25, 75–50, 100–75, 150–100
108-110	J2	17.85	71.21	30 Nov 20	1458	75–50, 100–75, 150–100
111-114	J3	17.91	71.21	1 Dec 20	1052	50–25, 75–50, 100–75, 150–100
115-118	M4	20.03	69.38	2 Dec 20	2016	50–25, 75–50, 100–75, 150–100
119-00	O2	22.41	67.8	4 Dec 20	953	150–100
120-123	O3	22.41	67.79	4 Dec 20	2011	50–25, 75–50, 100–75, 150–100
124-127	K3	9.11	75.72	12 Dec 20	2335	50–25, 75–50, 100–75, 150–100
128-131	K4	9.06	75.74	13 Dec 20	1507	50–25, 75–50, 100–75, 150–100
132-134	KK1	7.62	77.63	14 Dec 20	1226	50–25, 75–50
135-138	KK2	7.62	77.63	14 Dec 20	2047	50–25, 75–50, 100–75, 150–100
139-142	G4	15.32	73.21	3 Mar 22	823	50–25, 75–50, 100–75, 150–100
143-146	G5	15.68	73.21	4 Mar 22	1030	50–25, 75–50, 100–75, 150–100
147-150	M5	19.99	69.23	7 Mar 22	957	50–25, 75–50, 100–75, 150–100
151-154	O3	22.24	67.5	8 Mar 22	806	50–25, 75–50, 100–75, 150–100
155-158	U3	12.5	74.04	12 Mar 22	1156	50–25, 75–50, 100–75, 150–100
159-160	K4	9.04	75.42	13 Mar 22	1027	50–25, 75–50, 100–75
161-164	KK3	6.97	77.4	15 Mar 22	1220	50–25, 75–50, 100–75, 150–100

Table 3:

The mean, standard deviation at 40 and 104 m of biomass at 7 mooring sites and their difference is tabulated. All units are in $mg\ m^{-3}$.

	40 m		104 m		difference
	Mean	std	Mean	std	
Okha	230.42	22.84	151.68	25.58	78.74
Mumbai	272.86	34.95	182.24	30.34	90.62
Jaigarh	278.45	36.52	182.96	48.89	95.49
Goa	235.22	30.34	163.02	36.54	72.2
Udupi	247.81	34.37	169.37	38.8	78.43
Kollam	272.56	54.94	198.89	50.08	73.67
Kanyakumari	207.07	30.42	167.63	20.89	39.44

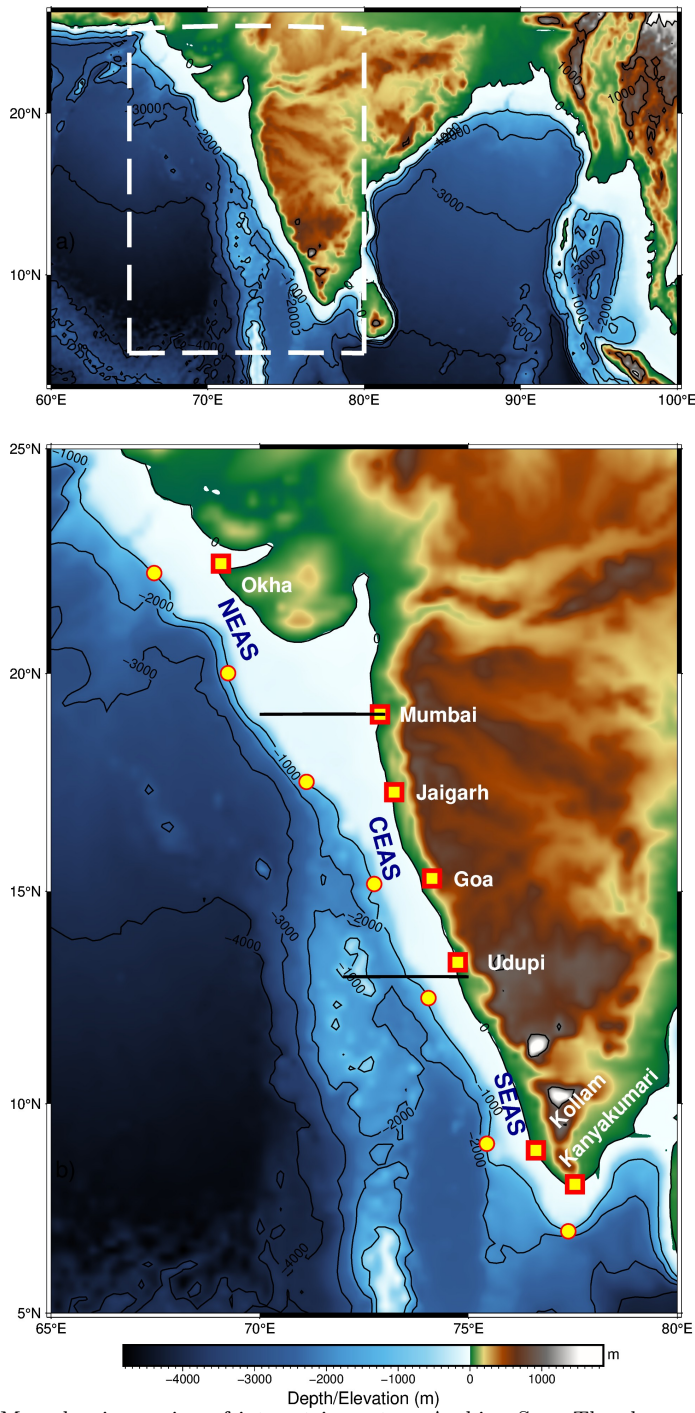


Figure 1: Map showing region of interest in eastern Arabian Sea. The slope moorings are deployed at ~ 1000 m depth as shown in the bathymetry contour. Note the increase in shelf width as we go poleward along the coast. The mooring sites off Okha and Mumbai are in Northern EAS; Jaigarh and Goa in Central EAS while Kollam and Kanyakumari are at Southern EAS. Udupi is situated at the transition zone of Central and Southern EAS.

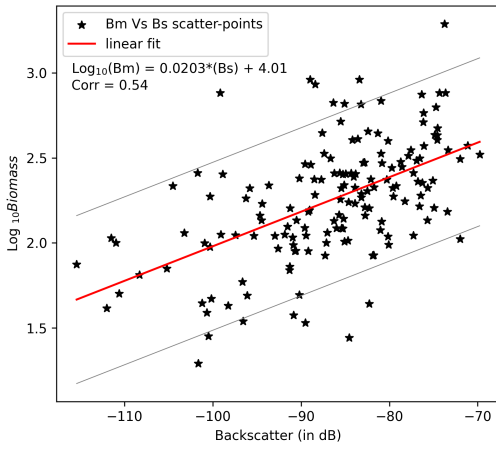


Figure 2: The linear fit line of Biomass (\log_{10} scale) and backscattering strength (in dB). The linear fit line is within the error range of previous result of [Aparna et al., 2022] (contained 67 data points) onto which latest zooplankton volumetric sample data (159 data points) is appended. The first standard deviation of \log_{10} Biomass is ± 0.49 , which results in the backscatter range of 48.58 dB encompassing the entire backscatter range. It signifies the robustness of zooplankton biomass dependency on ADCP measured backscattering strength.

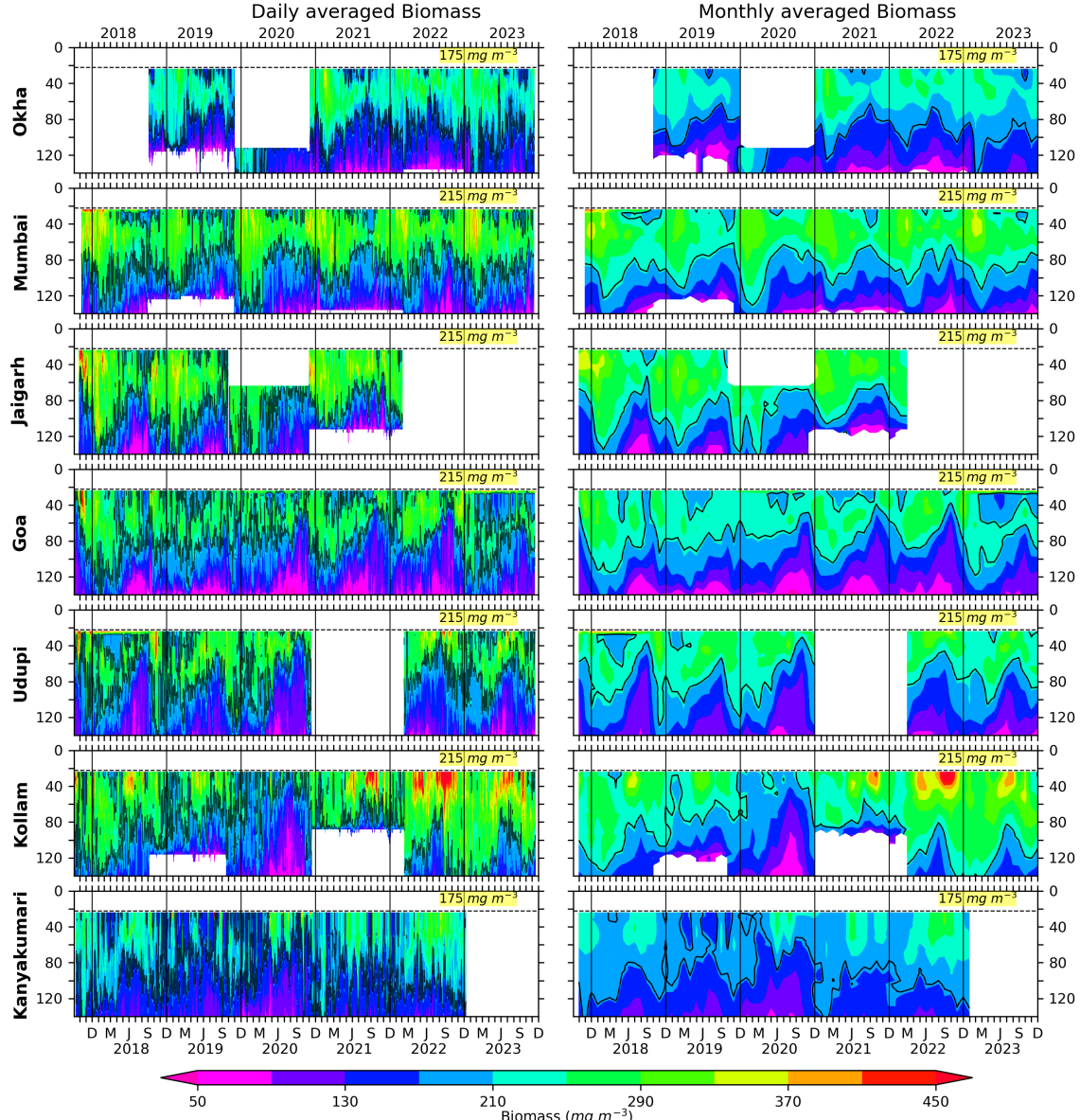


Figure 3: The Daily and monthly averaged biomass for EAS moorings, north (top) to south (bottom). The black contours are marking of 175 mg m^{-3} biomass for Okha and Kanyakumari; 200 mg m^{-3} for Jaigarh and Udupi; 215 mg m^{-3} for Mumbai, Goa and Kollam. The biomass contours are distinct and different based on the physico-chemical parameters and the one that best explains seasonality at respective location. The top 10 % of data is discarded due to echo noise. The dashed line at 22 m marks the top-depth of first bin i.e, 24 m.

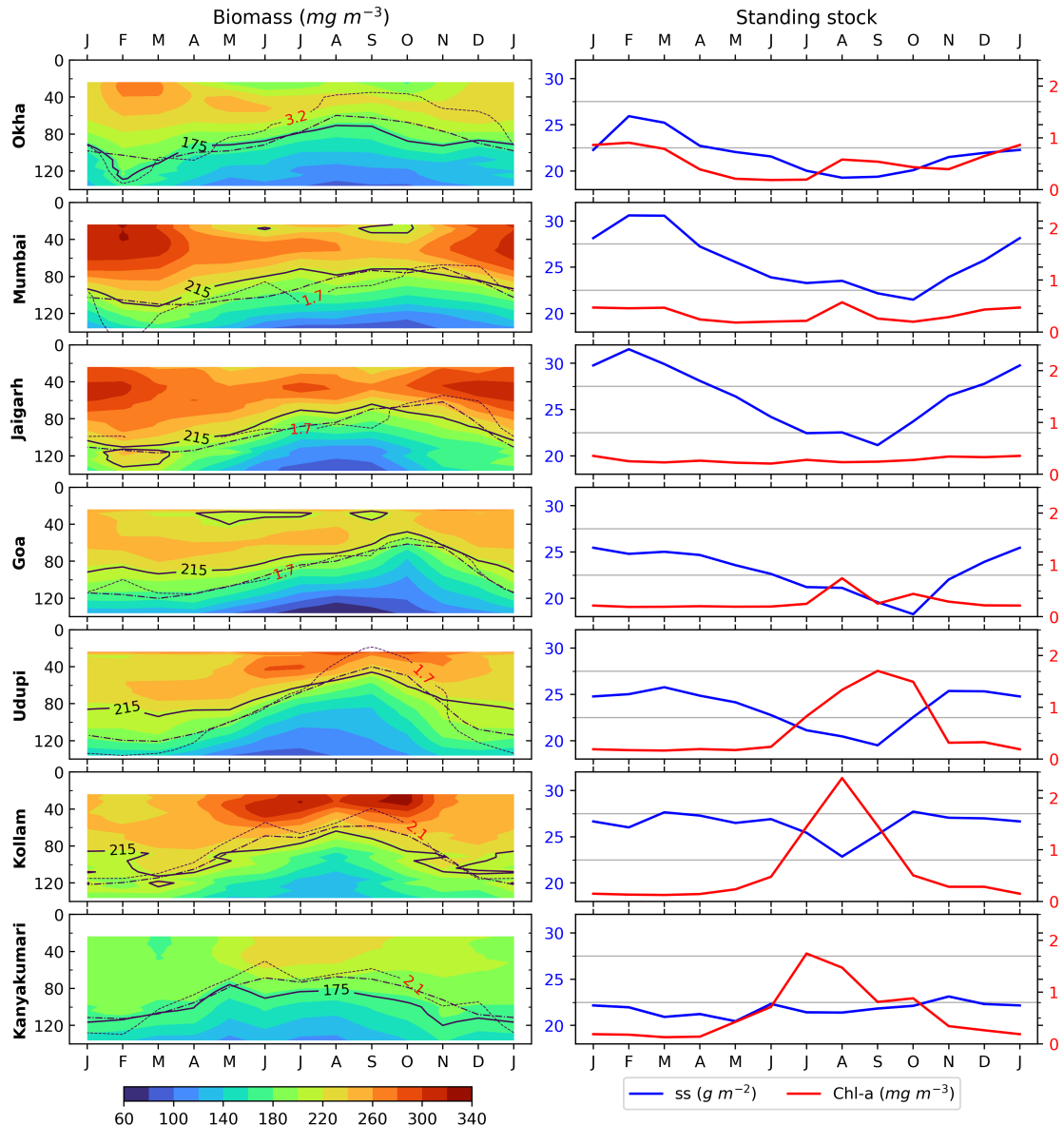


Figure 4: Monthly climatology of zooplankton biomass is shown in left panels for 7 locations, (top to bottom is southward). The D175, D200 & D215 are shown in solid lines; dashed line represents the depth of 23 C isotherm; oxygen contours are shown in dotted lines and labeled for each mooring. The right set of panel plots is showing ZSS and chlorophyll climatology for corresponding locations.

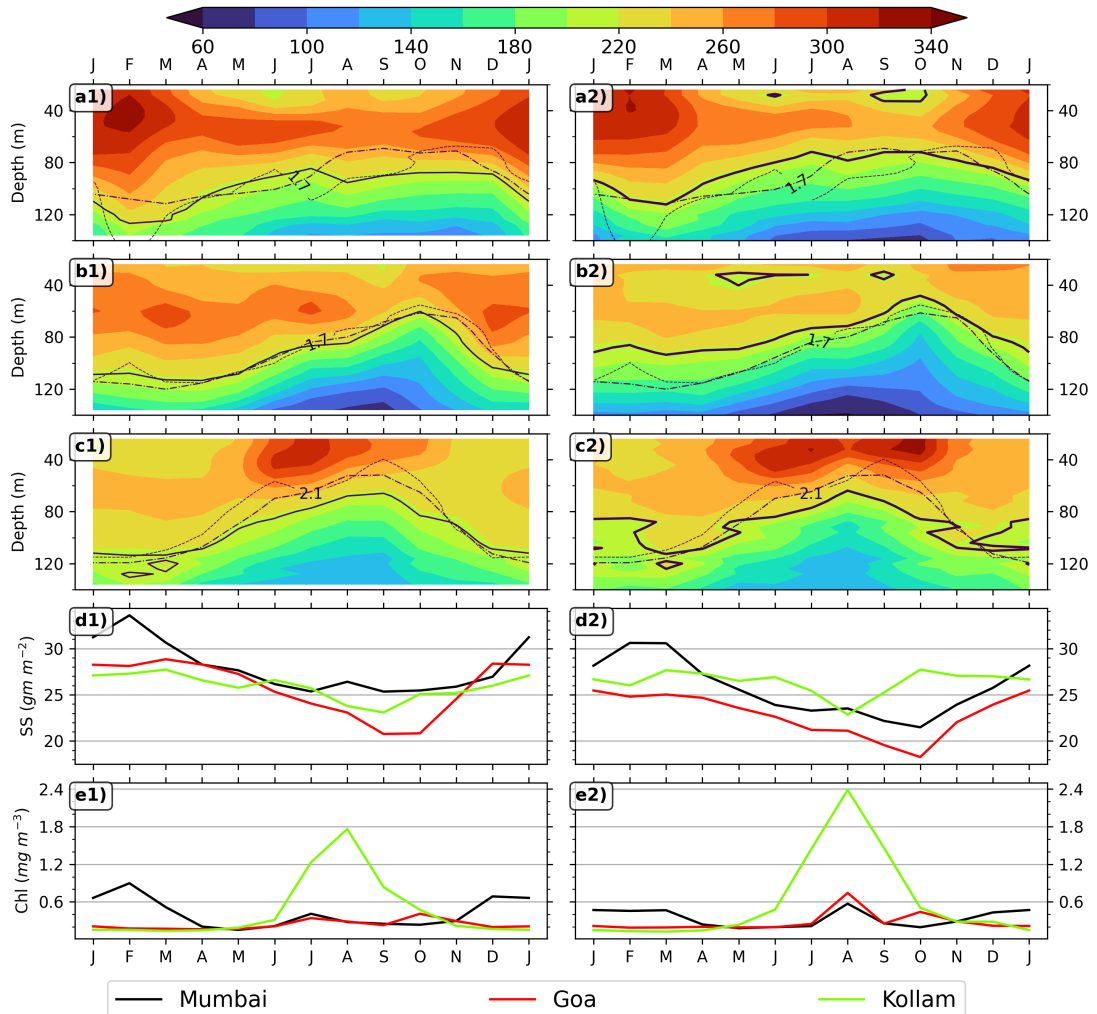


Figure 5: Monthly climatology of zooplankton biomass is shown in left panels for 3 locations which were earlier used in [Aparna et al., 2022]; a1, b1 & c1 is the biomass climatology for Mumbai, Goa and Kollam, d1 is for ZSS climatology, e1 is for chlorophyll biomass climatology; a2, b2, c2, d2 & e2 is same but based on data from 2017 to 2023. The D215 is shown in solid line. The dashed line represents the depth of 23 °C isotherm; oxygen contours are shown in dotted lines and labeled for each mooring.

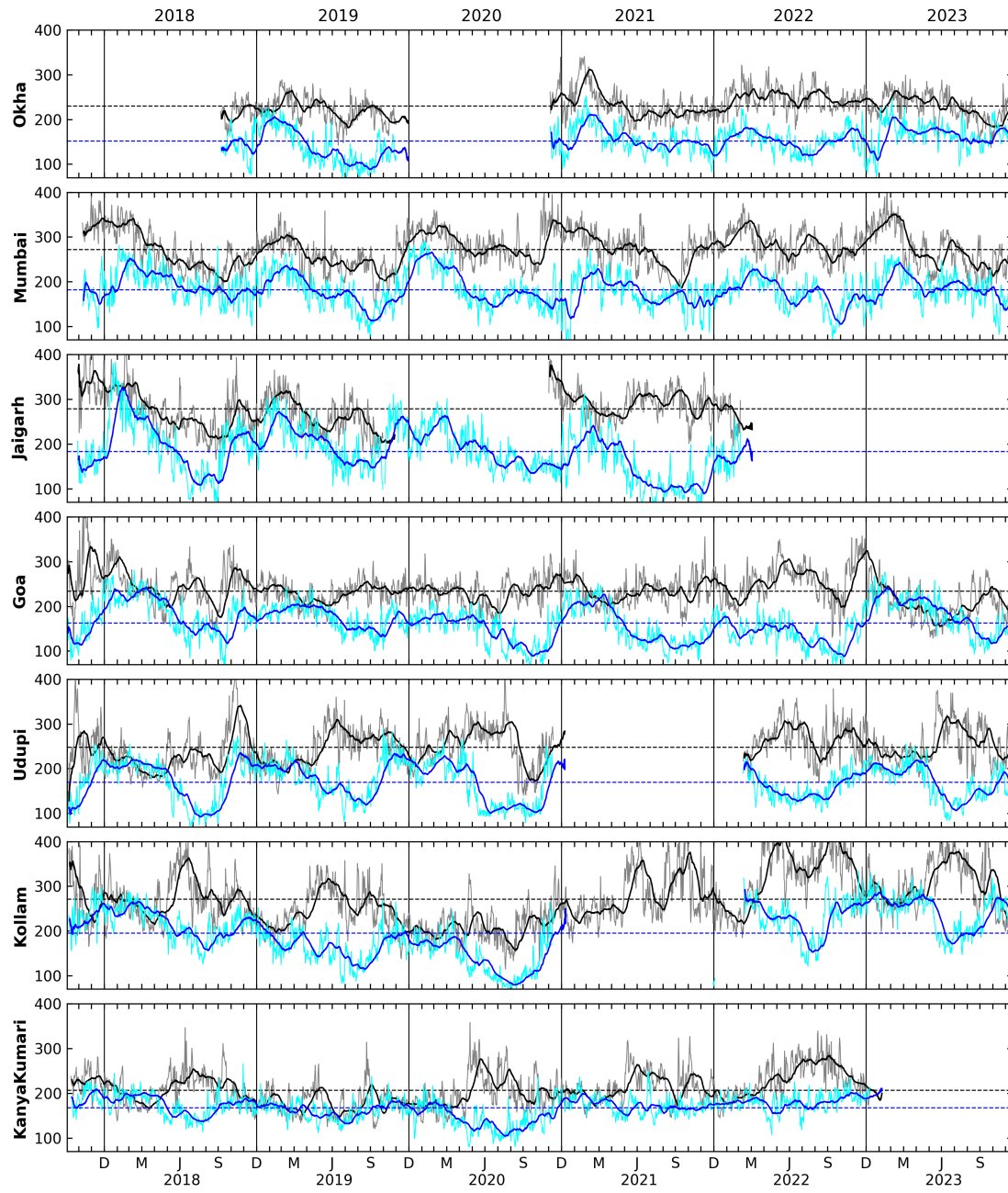


Figure 6: The daily biomass at depth of 40 m and 104 m for all locations shown by grey and cyan curves. The black and blue lines shows the 30 day rolling averaged biomass at 40 and 104 m, respectively. Notice the bursts seen in the daily data ranging from few days to weeks.

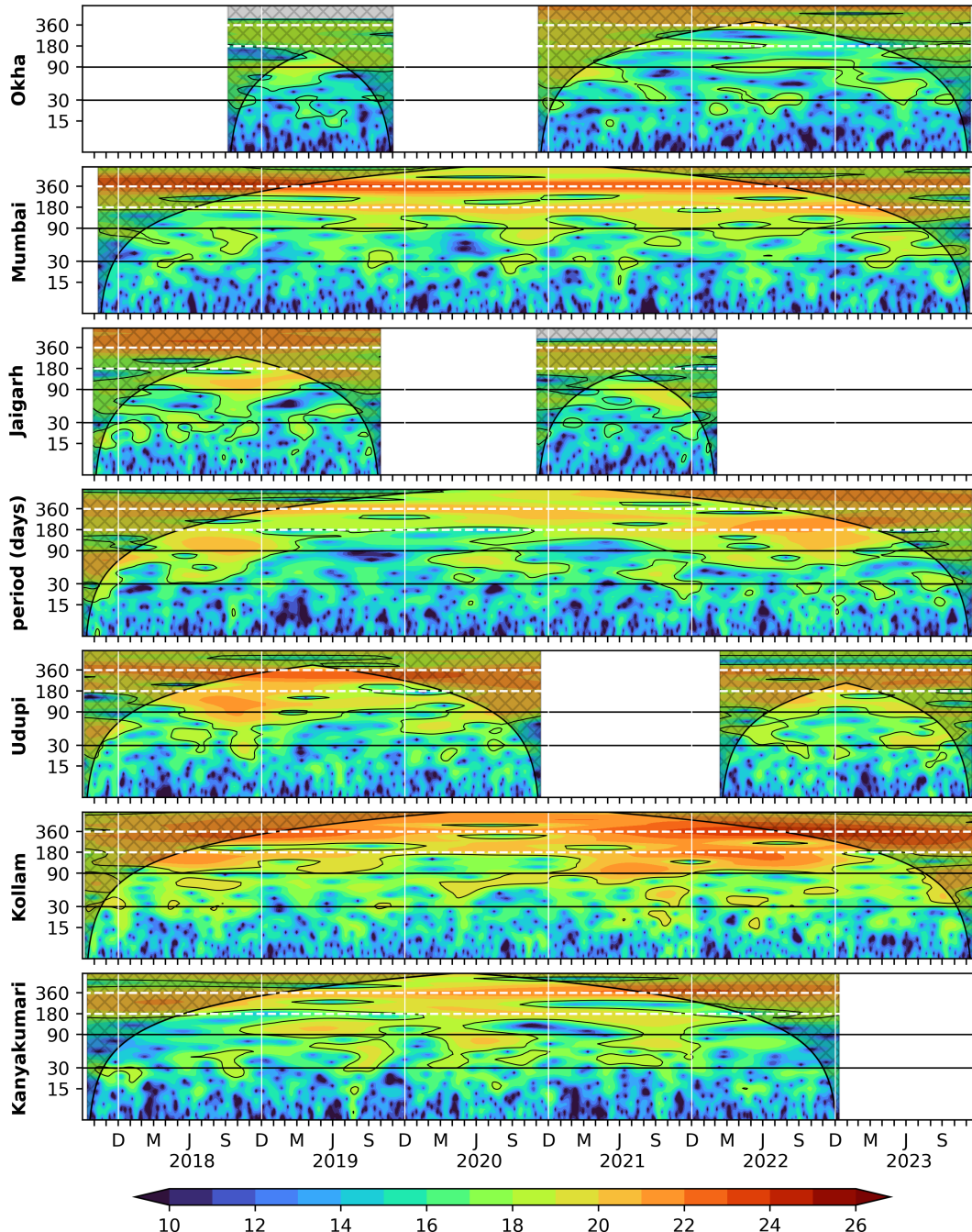


Figure 7: Wavelet power spectra (Morlet) of the 40 m zooplankton biomass plotted against time as abscissa and period in days as ordinate. The wavelet power is in \log_2 scale, the 95 % significance is marked in black contours; the cross-shaded region falls under cone of influence. Vertical white lines separates years.

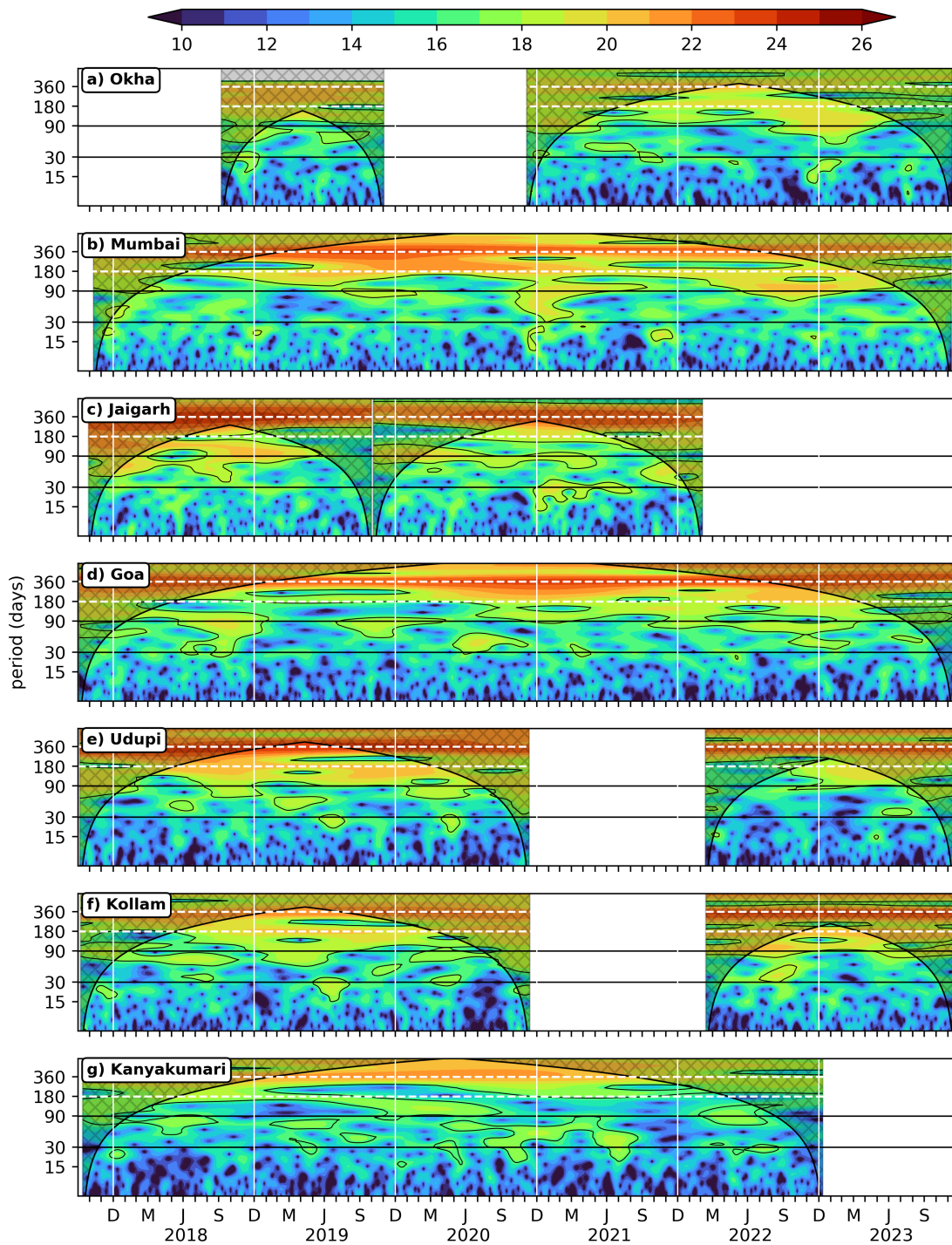


Figure 8: Wavelet power spectra (Morlet) of the 104 m zooplankton biomass plotted against time as abscissa and period in days as ordinate. The wavelet power is in log₂ scale, the 95 % significance is marked in black contours; the cross-shaded region falls under cone of influence. The vertical white lines separates years.

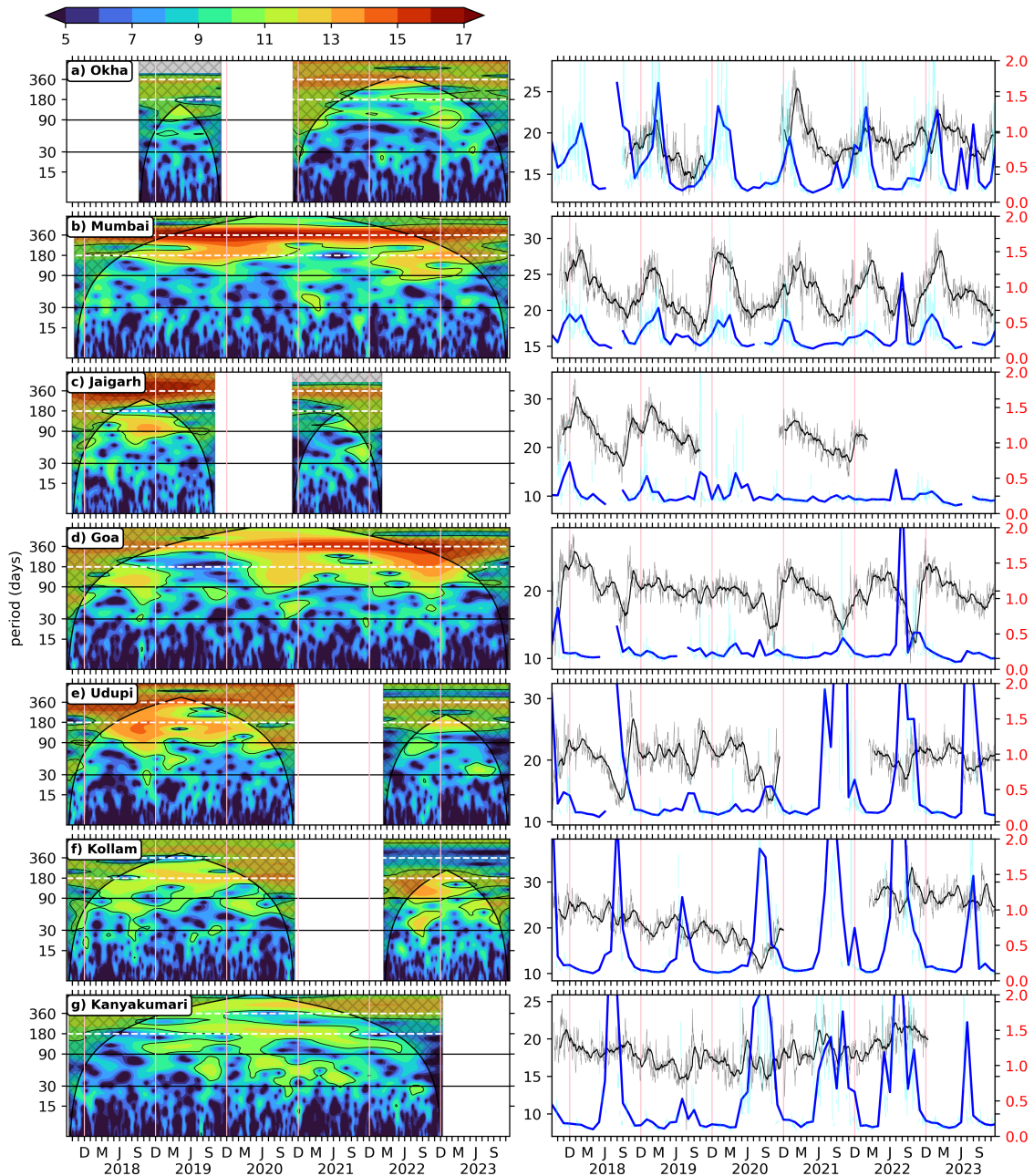


Figure 9: Wavelet power spectra (Morlet) of zooplankton standing stock plotted against time as abscissa and period in days as ordinate. The wavelet power is in log₂ scale, the 95 % significance is marked in black contours; The vertical white lines separates years. The right side panel shows the ZSS time series of 30 day rolling mean data (black)overlaid upon daily data (Grey). The 30 day rolling mean data of chlorophyll (solid blue line) is plotted over its daily data (cyan).

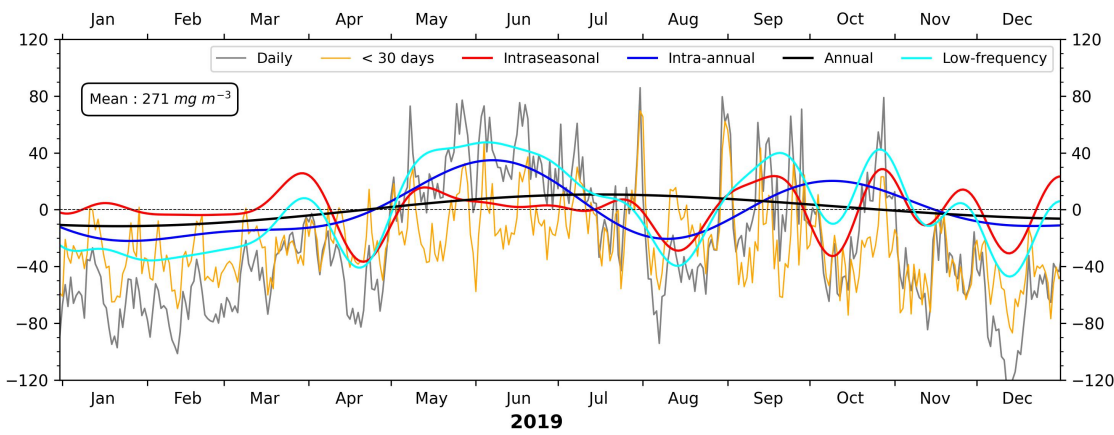


Figure 10: Comparison between mean-removed daily biomass time series at 40 m and the distinct components of variability off Kollam for 2019. The biomass units are mg m^{-3} . An increase in biomass is noticed from May onward and lasting till late monsoon with weeks of low biomass during August due to contribution from each component of variability. The cyan curve is sum of all low frequency components above 30 days, i.e, annual, intra-annual and 30 to 90 days intraseasonal variability.

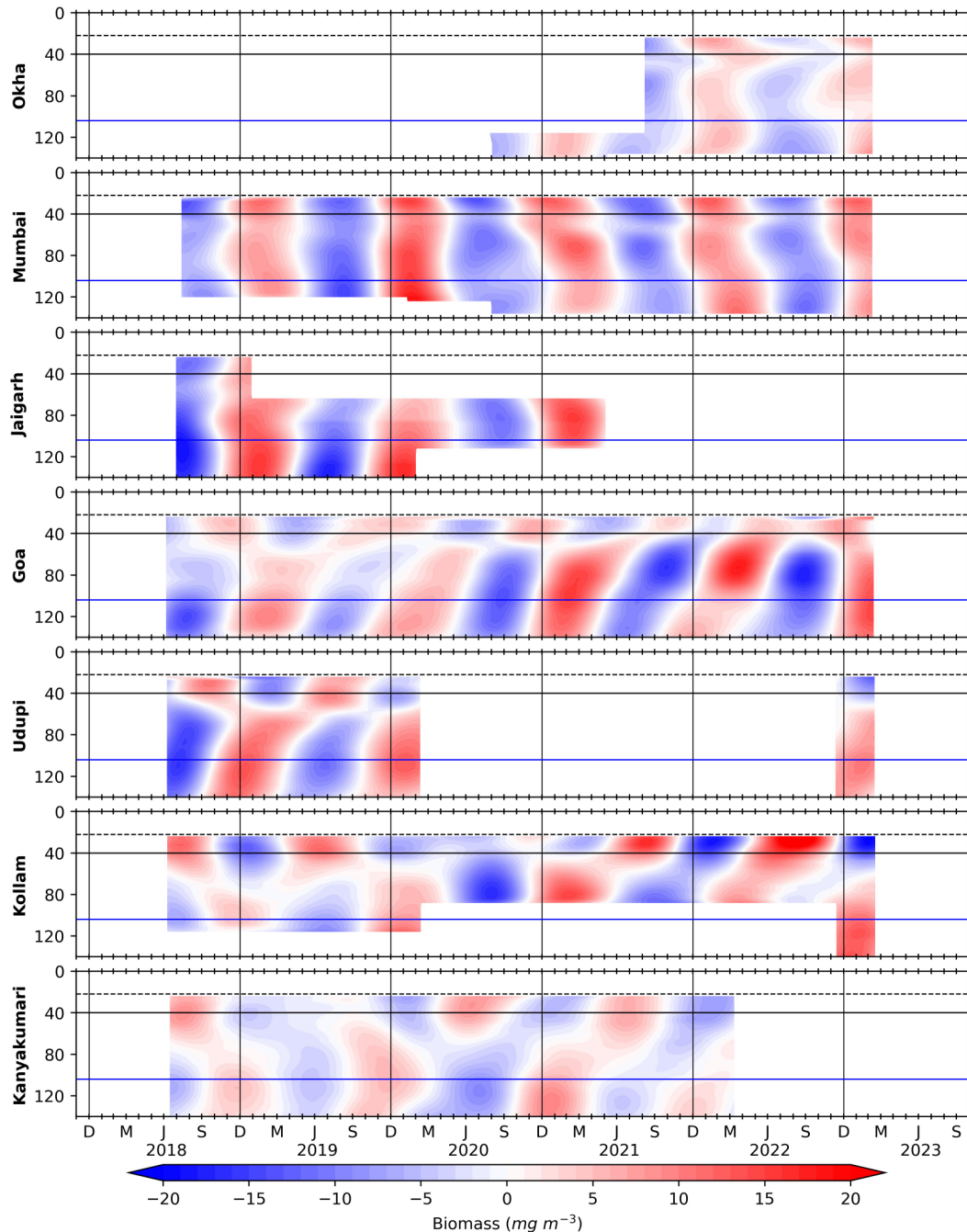


Figure 11: The biomass variation occurring in annual band (300 to 400 days). Owing to the presence of monsoon, there is a variation driven by associated upwelling (downwelling) processes in summer (winter) monsoon. and The horizontal black and blue lines is for 40 and 104 m respectively; vertical black lines separate the years. The dashed line at 22 m marks the top-depth of first bin i.e, 24 m.

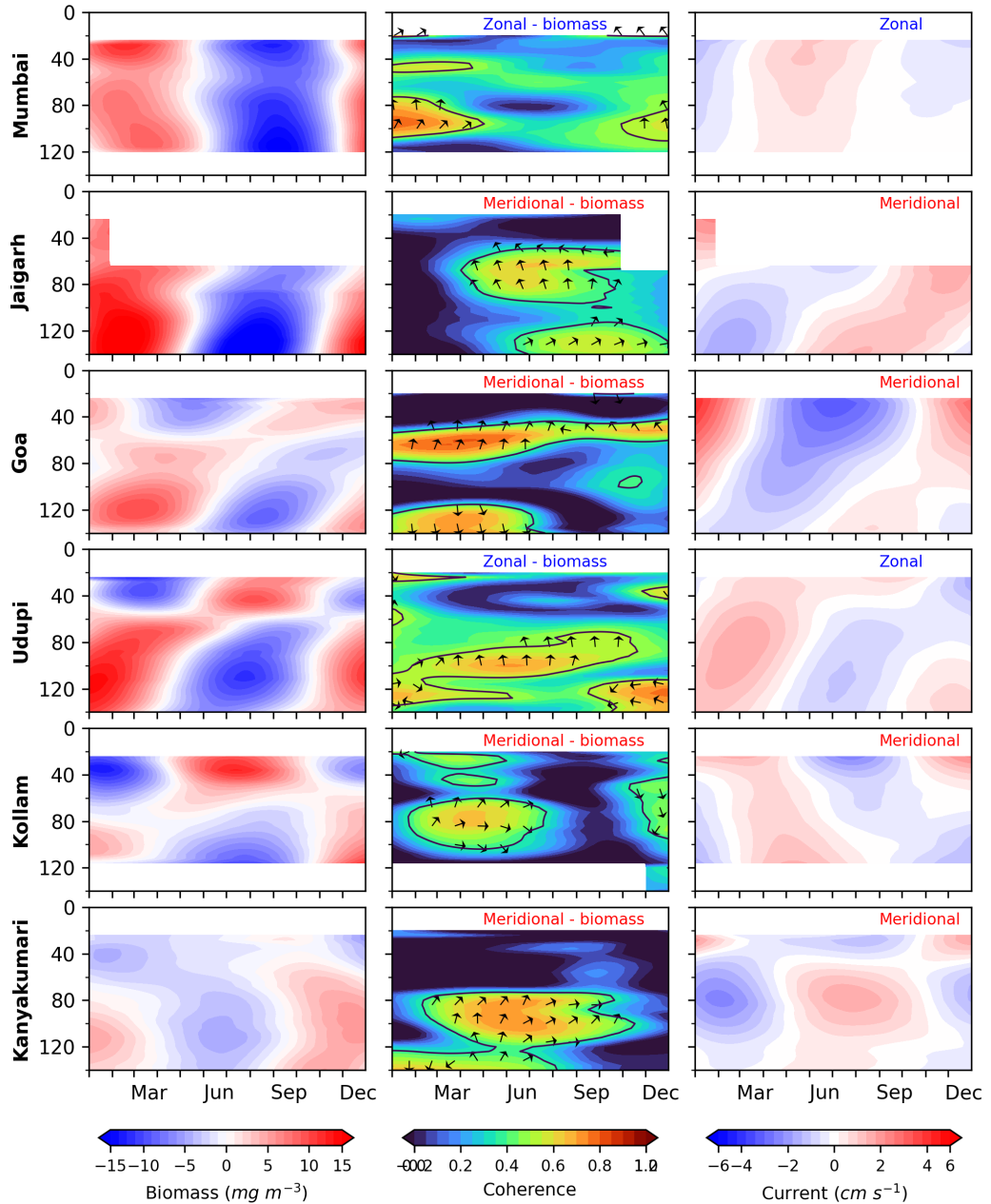


Figure 12: Current (zonal/meridional) and biomass wavelet coherence plotted alongside of annual filtered biomass and current. Either zonal or meridional current is considered depending on coherence and if current leads biomass. The solid contour encompasses greater than 0.5 coherence and phase is plotted with north as reference, +ve (-ve) x-axis is current leading (lagging) biomass. Left (Right) panel is for biomass (current). Although the annual biomass variability is weak and contributes less to the total biomass time series, upward phase propagation is seen implying upwelling favorable conditions leading to biomass growth.

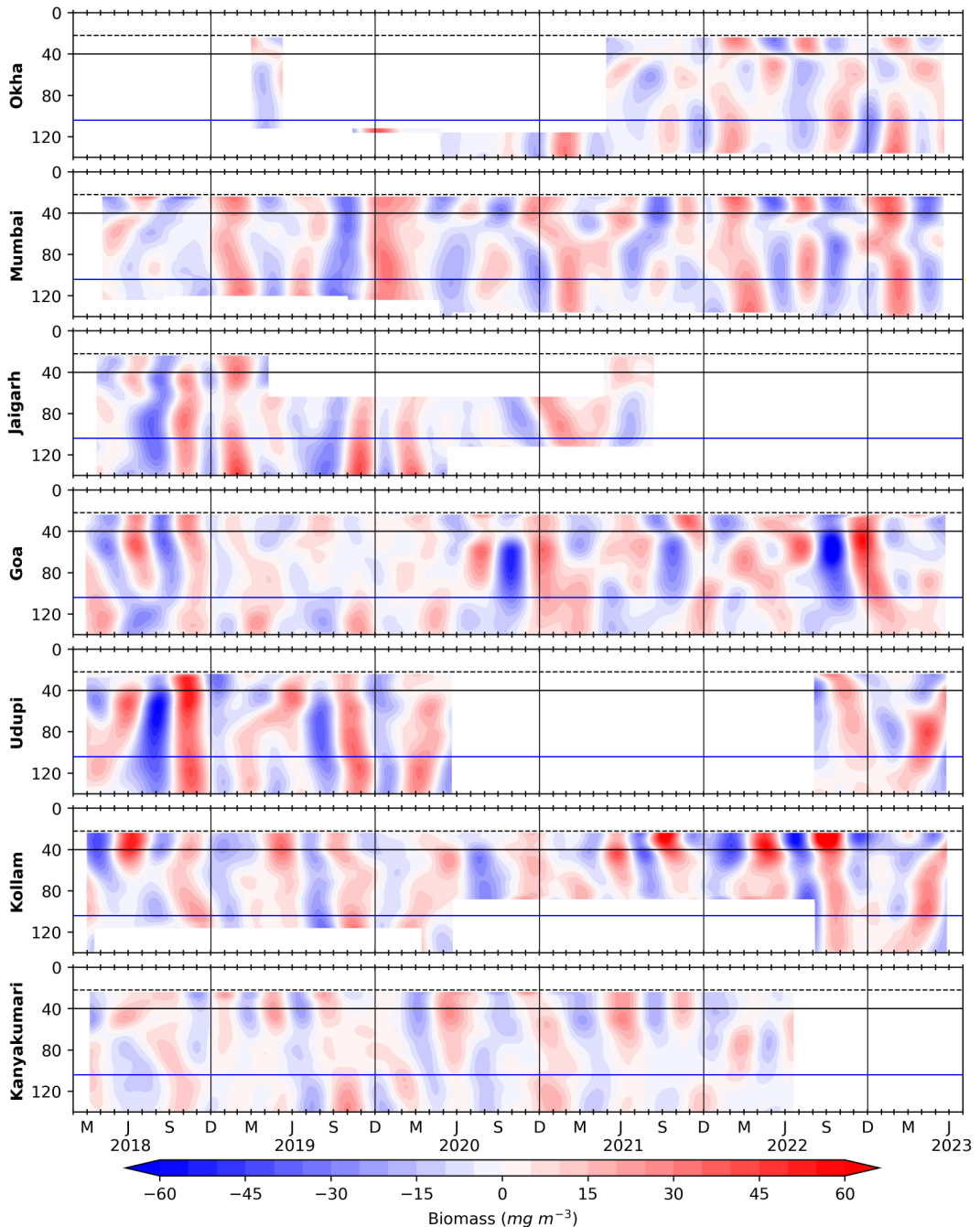


Figure 13: The biomass variation occurring in 100 to 250 days period (between the seasons and within a year record or intra-annual band) is obtained using a band pass filter. The horizontal black and blue lines is for 40 and 104 m respectively; vertical black lines separate the years. The dashed line at 22 m marks the top-depth of first bin i.e, 24 m.

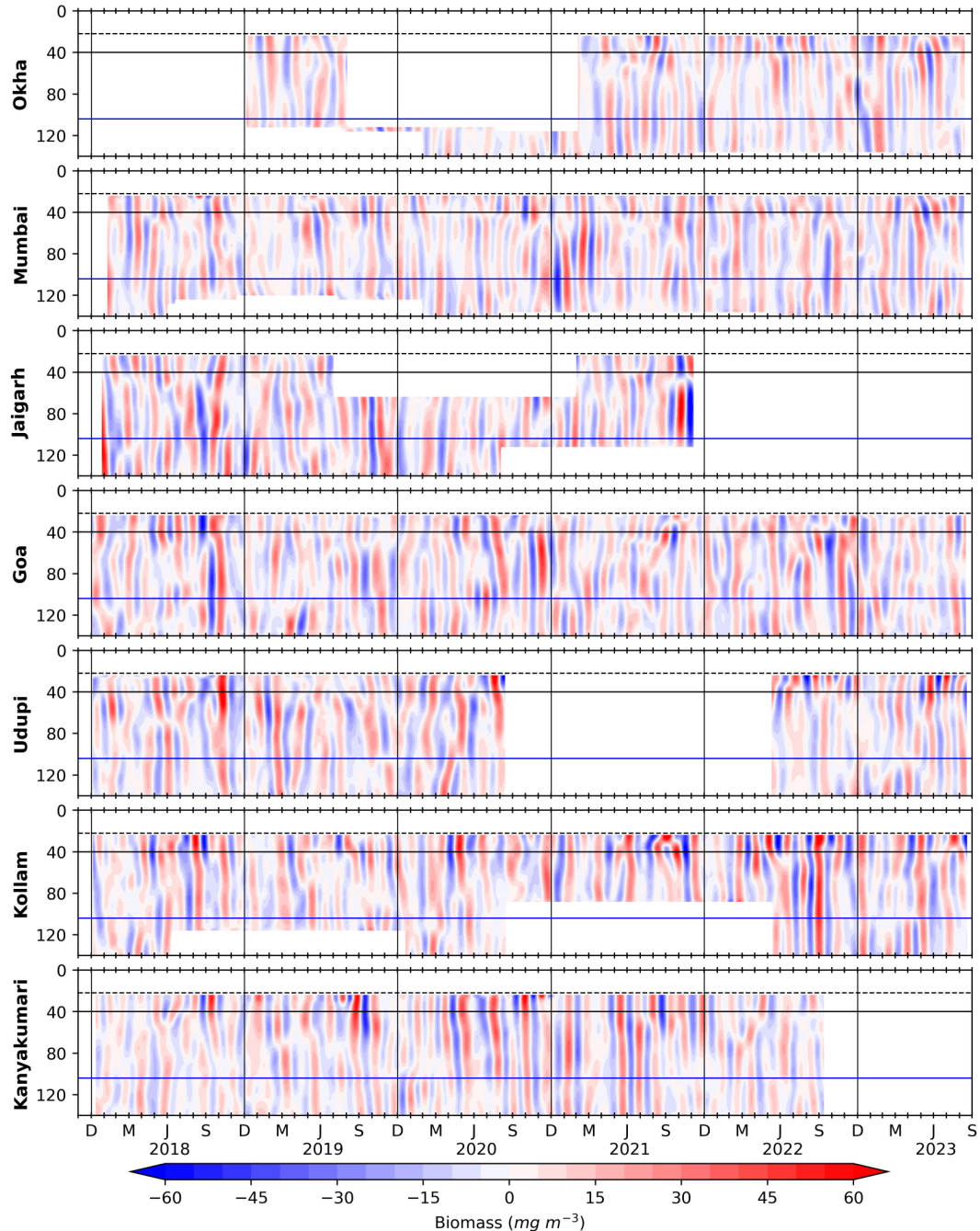


Figure 14: Biomass variation found in the scale of 30 to 90 days period (Intra-seasonal band as it is within a season) is obtained using a lanczos band pass filter. The horizontal black and blue lines is for 40 and 104 m respectively; vertical black lines separate the years. The dashed line at 22 m marks the top-depth of first bin i.e, 24 m. Intraseasonal variability is seen throughout the record and the variability is stronger during August to November.